Cortical gene expression architecture links healthy neurodevelopment to the imaging, transcriptomics, and genetics of autism and schizophrenia

Richard Dear, Konrad Wagstyl, Jakob Seidlitz, Ross D. Markello, Aurina Arnatkevičiūtė, Kevin M. Anderson, Richard A.I. Bethlehem, Lifespan Brain Chart Consortium, Armin Raznahan, Edward T. Bullmore, Petra E. Vértes

Affiliations

Department of Psychiatry, University of Cambridge, Cambridge, UK
Richard Dear, Richard A.I. Bethlehem, Edward T. Bullmore, Petra E. Vértes
Lifespan Brain Institute, The Children's Hospital of Philadelphia and Penn Medicine, Philadelphia, PA, USA
Jakob Seidlitz
Department of Child and Adolescent Psychiatry and Behavioral Science, The Children's Hospital of Philadelphia, Philadelphia, PA, USA
Jakob Seidlitz
Department of Psychiatry, University of Pennsylvania, Philadelphia, PA, USA
Jakob Seidlitz
McConnell Brain Imaging Centre, Montreal Neurological Institute, McGill University, Montreal, Quebec, Canada
Ross D. Markello
Turner Institute for Brain and Mental Health, Monash University, Melbourne, Australia
Aurina Arnatkevičiūtė
Department of Psychology, Yale University, New Haven, CT, USA
Kevin M. Anderson
Wellcome Centre for Human Neuroimaging, London, UK
Konrad Wagstyl
Section On Developmental Neurogenomics, National Institute of Mental Health, Bethesda, MD, USA
Armin Raznahan
Lifespan Brain Chart Consortium

List of members https://github.com/brainchart/Lifespan

Corresponding author:

Richard Dear, rajd2@cam.ac.uk

Abstract

Human brain organisation involves the coordinated expression of thousands of genes. For example, the first principal component (C1) of cortical transcription identifies a hierarchy from sensorimotor to association regions. Here, optimised processing of the Allen Human Brain Atlas revealed two new components of cortical gene expression architecture, C2 and C3, which are distinctively enriched for neuronal, metabolic and immune processes, specific cell-types and cytoarchitecture, and genetic variants associated with intelligence. Using additional datasets (PsychENCODE, Allen Cell Atlas, and BrainSpan), we found that C1-C3 represent generalisable transcriptional programmes that are coordinated within cells, and differentially phased during foetal and postnatal development. Autism spectrum disorder and schizophrenia were specifically associated with C1/C2 and C3, respectively, across neuroimaging, differential expression, and genome-wide association studies. Evidence converged especially in support of C3 as a normative transcriptional programme for adolescent brain development, which can lead to atypical supra-granular cortical connectivity in people at high genetic risk for schizophrenia.

Main Text

Introduction

How does the complex anatomical and functional organisation of the human brain develop from the expression of over twenty thousand genes [1]? And how does this process go awry in neurodevelopmental disorders? In the last 10 years, whole-brain, whole-genome transcriptional atlases, such as the Allen Human Brain Atlas (AHBA) [2], have suggested that healthy brain organisation may depend on "transcriptional programmes" representing the coordinated expression of large numbers of genes over development [3–7].

In 2012, Hawrylycz *et al.* showed that principal components of the AHBA dataset capture distinct features of cortical anatomy [2]. In 2018, Burt *et al.* argued that the first principal component of cortical gene expression (C1) reflects an anterior-to-posterior "neuronal hierarchy", defined in macaque tract-tracing data by feedforward and feedback axonal connections between cortical areas [8–10] and indexed in humans by the ratio of T1- and T2-weighted MRI signals, a putative marker of cortical myelination [8]. These discoveries echoed prior findings from studies of embryonic development of chick, mouse and human brains where spatially patterned transcriptional gradients have been shown to organise neurodevelopmental processes such as areal differentiation, axonal projection, and cortical lamination [6,11–13]. Single-cell RNA sequencing data has also revealed an anterior-to-posterior gradient in the gene expression of inhibitory interneurons, which is conserved across multiple species including humans [14]. It is therefore likely that the principal component of gene expression in the adult human cortex represents a transcriptional programme key to its normative development.

However, it is not clear that C1 is the only component of spatially patterned and neurodevelopmentally coordinated gene expression in the human brain. Hawrylycz *et al.* suggested that principal component analysis (PCA) of a restricted set of 1,000 genes in one of the six brains of the AHBA dataset revealed multiple biologically-relevant components [2] (**Supplementary Fig. S1**). Later, Goyal *et al.* used nonlinear dimension reduction across whole-genome spatial expression, again from only one of the six AHBA brains, to show that aerobic glycolysis was associated with a second transcriptional component [15]. To our knowledge, more recent studies using all available AHBA data have reliably found only C1 [8,16]. This first component has been linked to a general "sensorimotor-association axis" of brain organisation [10] derived from several macro-scale brain phenotypes, including among others the principal gradient of functional connectivity [17], maps of brain metabolism and blood flow [15], and the map of human cortical expansion compared to other primates [18]. Although it is

parsimonious to assume that such diverse brain phenotypes could all be determined by a single transcriptional programme, it seems more realistic to expect that multiple transcriptional programmes are important for human brain development, as is generally the case for brain development in other species [19].

Here we present two higher-order components of human cortical gene expression, C2 and C3, that likely represent additional transcriptional programmes distinct from the C1 component already reliably described [8]. These higher-order components only emerged when optimised data-filtering and dimension-reduction methods were applied to the AHBA dataset. We found that C2 and C3 are each specifically enriched for biologically-relevant gene sets, and spatially co-located with distinct clusters of neuroimaging phenotypes or macro-scale brain maps. Leveraging independent RNA sequencing datasets on single-cell and developmental gene expression, we further demonstrated that all three components are generalisable to other datasets, representative of coordinated transcription within cells of the same class, and dynamically differentiated over the course of foetal, childhood and adolescent brain development. Finally, by triangulating evidence across case-control neuroimaging, differential gene expression, and genome-wide association studies (GWAS), we demonstrated that components C1 and C2 are specifically associated with autism spectrum disorder (ASD), and C3 with schizophrenia. While prior studies have used the AHBA to derive gene sets correlated with disorder-related MRI phenotypes [20–25], this disorder-first, "imaging transcriptomics" [26–28] approach is susceptible to identifying genes whose co-location with MRI phenotypes reflects secondary associations or consequences of a disorder, such as behavioural changes (e.g. smoking, alcohol use), physical health disorders (e.g. obesity, diabetes), or pharmacological treatment [29–31]. What is of most interest for neurodevelopmental disorders is to understand the pathogenic provenance of a clinically diagnosable disorder – to ask "what developed differently?" rather than merely "what is different?". Our approach sought to distinctively address the question of what "develops differently" based on an understanding of "normal development", by linking genetic risks and atypical phenotypes to a generalisable transcriptional architecture of healthy brain development.

114 **Results**

115 Three components pattern cortical gene expression

116 We first applied PCA to the entire AHBA dataset of 6 adult brains [2]. Microarray measurements of
117 relative messenger RNA levels were processed to represent mean expression of ~16,000 genes at
118 each of the 180 regions of the left hemispheric cortex defined by the HCP-MMP parcellation [32–34]
119 (**Methods**). We initially found that higher-order components (C2, C3) estimated by PCA of the
120 resulting {180 × 16,000} data matrix were not robust to sampling variation of the six donor brains,
121 with low generalisability, g, compared to C1: $g_{C1} = 0.78$, $g_{C2} = 0.09$, $g_{C3} = 0.14$ (**Methods**). However, two
122 data processing improvements were found to enhance the generalisability of higher order
123 components. First, we optimised the trade-off involved in excluding noisy data – by filtering spatially
124 inconsistent genes (with low differential stability [35]) and under-sampled brain regions – while seeking
125 to maximise the anatomic and genomic scope of the data matrix (**Extended Data Fig. 1**). Second, we
126 used the non-linear dimension reduction technique of diffusion map embedding (DME), instead of
127 linear PCA, to identify coordinated gene expression patterns from the matrix. DME is robust to noise
128 and more biologically plausible than PCA in this context because of its less strict orthogonality
129 constraints (**Methods**). We found that while PCA and DME both identified the same components from
130 the filtered gene expression matrix (**Extended Data Fig. 1d**), using DME was necessary to achieve high
131 generalisability g while also retaining sufficient genes for downstream enrichment analyses.
132
133 We applied DME to the (137 × 7,937} filtered AHBA data matrix comprising the expression of the 50%
134 most stable genes measured in the 137 cortical areas with data available from at least three brains.
135 The generalisability of the first three components was substantially increased, i.e., $g_{C1} = 0.97$, $g_{C2} =$
136 0.72, $g_{C3} = 0.65$, while the generalisability of even higher-order components remained low, e.g., $g_{C4} =$
137 0.28 (**Fig 1a**). We found that the cortical maps of C2 and C3 derived from DME on filtered data were
138 more spatially smooth than the corresponding PCA-derived maps on unfiltered data (**Fig. 1b**),
139 consistent with higher generalisability indicating less contamination by spatially random noise. C1-C3
140 were also robust to variations in parameters for processing the AHBA, including choice of parcellation
141 template (**Extended Data Fig. 2**). Finally, the transcriptional patterns represented by C1-C3 in the
142 AHBA dataset were reproducible in an independent PsychENCODE dataset comprising bulk RNA-seq
143 measurements of gene expression at 11 cortical regions from N=54 healthy controls [36] (regional
144 correlation $r_{C1} = 0.85$, $r_{C2} = 0.75$, $r_{C3} = 0.73$; see **Extended Data Fig. 3** and **Supplementary Table S5**).
145
146

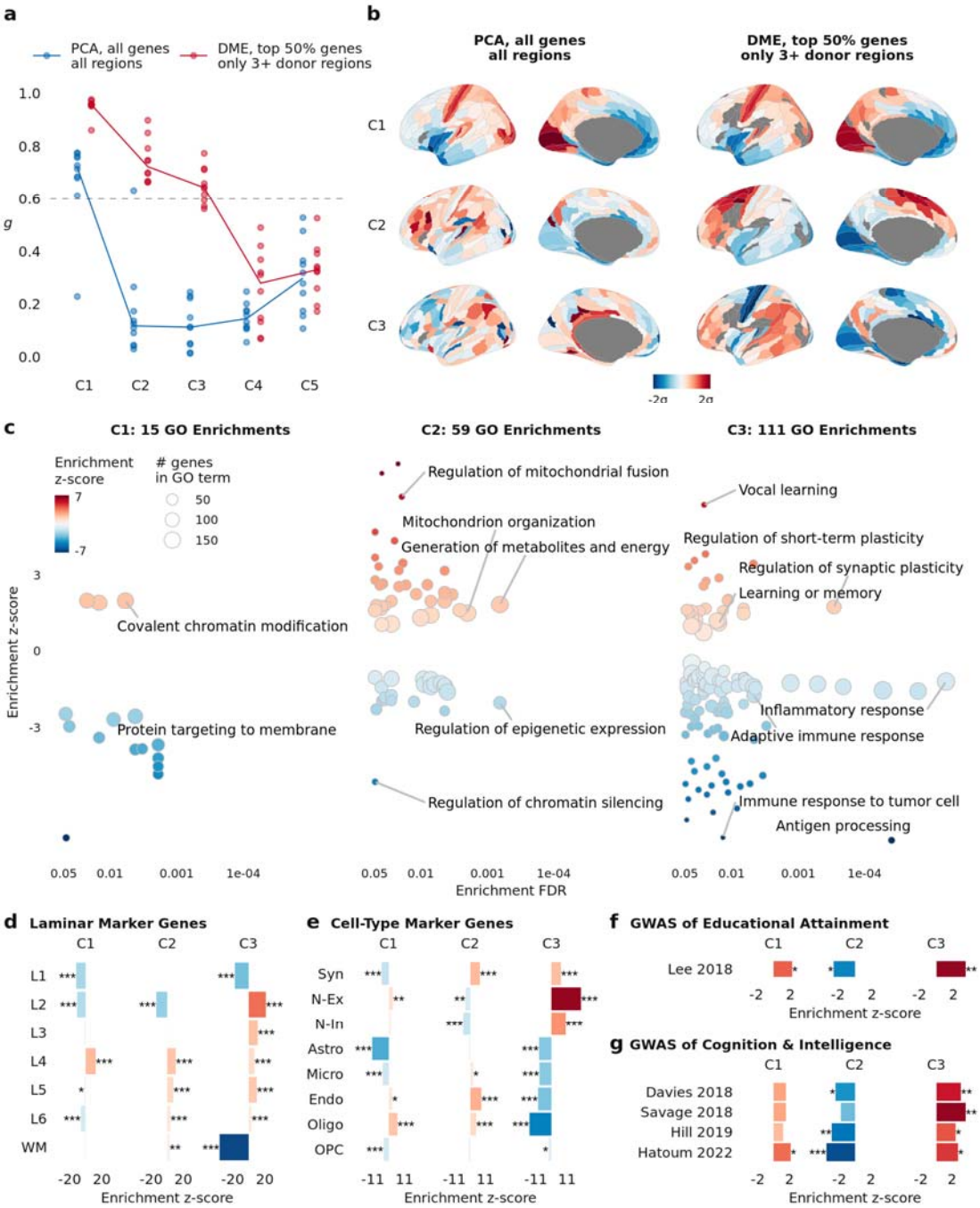

***Figure 1**: Three generalisable components of human cortical gene expression were enriched for biological processes, cytoarchitecture, and cognitive capacity. **a**, To identify robust components of cortical gene expression, we split the six-brain AHBA dataset into two disjoint triplets of three brains, applied PCA to each triplet, and correlated the resulting matched components (C1, C2, C3…) (Methods). For each component, the median absolute correlation over all 10 permutations of triplet pairs was a proxy for its generalisability, g. Using PCA and previously published best practices for processing the AHBA dataset [33,34], generalisability decreased markedly beyond the first component: $g_{C1} = 0.78$, $g_{C2} = 0.09$, $g_{C3} = 0.14$ (**Fig. 1a**). Using diffusion map embedding (DME) with the top 50% most stable genes, and the 137 regions with data available from at least three brains,*

*the generalisability of the first three components substantially increased: g_{C1} = 0.97, g_{C2} = 0.72, g_{C3} = 0.65 (**Fig 1a**). **b**, Cortical maps of brain regional scores of components C1-C3 estimated by DME on the filtered AHBA dataset displayed smooth spatial gradients (right; Moran's I [37] 0.48, 0.58, and 0.21 for C1-C3 respectively), unlike those of PCA on the unfiltered data (left; Moran's I 0.50, 0.09 and 0.07). **c**, Gene Ontology Biological Process enrichments for C1-C3 showed that the number of significant enrichments was greater for higher-order components, illustrating that they were more biologically specific. C2-positive genes were enriched for metabolism while C2-negative genes were enriched for regulatory processes; C3-positive genes were enriched for synaptic plasticity and learning while C3-negative genes were enriched for immune processes. **d,** C1-C3 were distinctively enriched for marker genes of six cortical layers and white matter (WM) [38]. **e**, C1-C3 were also distinctively enriched for marker genes of cell types and synapses [44]. **f**, All three components were significantly enriched for genes mapped to common variants associated with educational attainment in prior GWAS data [39]. **g**, C2 and C3 (but not C1) were significantly enriched for genes mapped to common variation in intelligence and cognition across four independent GWAS studies [40–43]. For d-g, significance was computed by two-sided permutation tests (Methods) and FDR-corrected across all tests in each panel; *, **, *** respectively indicate FDR-corrected two-sided p-values: 0.05, 0.01, 0.001.*

The first three DME components, C1-C3, explained 38%, 10%, and 6.5%, respectively, of the total variance of the filtered AHBA dataset (**Methods**). The proportion of variance explained was related to the number of genes that were strongly weighted (absolute correlation $|r| \geq 0.5$) on each component: 4,867 genes (61%) were strongly weighted on C1, 967 genes (12%) on C2, and 437 genes (5.5%) on C3 (**Supplementary Fig. S2**). The three components also had distinct axial alignments in anatomical space, and the co-expression network of cortical regions displayed clear anatomical structure even when the highest-variance C1 component was regressed out (**Extended Data Fig. 4**). These findings demonstrate that these three expression patterns shared across hundreds to thousands of genes are likely to be biologically relevant.

To interpret the DME-derived components in more detail, we first used enrichment analyses of the weights of the 7,973 genes on each component (**Methods**). Many more Gene Ontology (GO) Biological Process terms were significantly enriched (with false discovery rate [FDR] = 5%) for C2 (59 GO terms) and C3 (111 GO terms) than for C1 (15 GO terms) (**Fig. 1c**).

Although C1 was enriched for relatively few, functionally general biological processes, it precisely matched the first principal component previously reported (r = 0.96) [8]. The same interneuron marker genes (*SST*, *PVALB*, *VIP*, *CCK*) and glutamatergic neuronal genes (*GRIN* and *GABRA*) were strongly weighted with opposite signs (positive or negative) on C1 (**Supplementary Fig. S3**).

For genes positively-weighted on C2, 23 of 36 enrichments were for metabolic processes, and for negatively-weighted genes, 19 of 23 enrichments were for epigenetic processes (**Fig. 1c, Supplementary Table 2**). Whereas, for genes positively-weighted on C3, 19 of 27 enrichments were related to synaptic plasticity or learning, and for negatively-weighted genes, 33 of 84 enrichments involved the immune system. We further analysed enrichment for genes identified as markers of specific cortical layers [38] (**Fig. 1e**) and cell types [44] (**Fig. 1f**), and in each case observed distinct enrichment profiles for C1-C3. For example, genes positively-weighted on C3 were enriched for marker genes of neurons, synapses, and cortical layers 2 and 3 (L2, L3), whereas genes negatively-weighted on C3 were enriched for glial (especially oligodendroglial) marker genes.

We also explored the biological relevance of the three components by enrichment tests for genes associated with variation in adult cognitive capacity. We found that all three components C1-C3 were enriched for genes significantly associated with educational attainment (**Fig. 1f**) [39]. Across four independent GWAS studies of intelligence and cognition [40–43], genes strongly weighted on C1 were not significantly enriched, but genes negatively-weighted on C2 were enriched for genetic variants associated with intelligence in three of the four studies, and genes positively-weighted on C3 were enriched for genes identified by all four prior GWAS studies of intelligence (**Fig. 1g**).

Neuroimaging maps align to three transcriptional components

Prior work has linked gene transcription to a multimodal "sensorimotor-association axis" (S-A axis) [10] of brain organisation, defined as the composite of 10 brain maps, comprising the first principal component of gene expression (C1) and 9 other MRI or PET neuroimaging maps that were selected to differentiate sensorimotor and association cortices. We first aimed to build on this work by analysing the correlation matrix of the same set of 9 brain maps together with the three transcriptional components derived from DME of the filtered AHBA dataset. Data-driven cluster analysis of this {12 x 12} correlation matrix identified three clusters, each including one of the orthogonal transcriptional components (**Fig. 2a, Methods**). C1 was clustered together with 2 MRI maps: the T1w/T2w myelination marker [45] and cortical thickness [46]; C2 was clustered with 5 maps: aerobic glycolysis [47], cerebral blood flow [48], cortical expansion in humans relative to non-human primates [18], inter-areal allometric scaling [49] and external pyramidal cell density [50]; and C3 was clustered with 2 maps: the principal gradient of fMRI connectivity [17] and first principal component of cognitive terms meta-analysed by Neurosynth [51]. While some maps were specifically aligned to one component, e.g. aerobic glycolysis r_{C2} = 0.66 (p_{spin} = 0.004, FDR < 5%), others were moderately correlated with multiple transcriptional components, e.g., for cerebral blood flow: r_{C1} = 0.25, r_{C2} = 0.28 and r_{C3} = 0.33. This

clustering analysis suggests that it is overly parsimonious to align all 9 neuroimaging phenotypes with just one transcriptional component (C1) as part of a singular sensorimotor-association cortical axis.

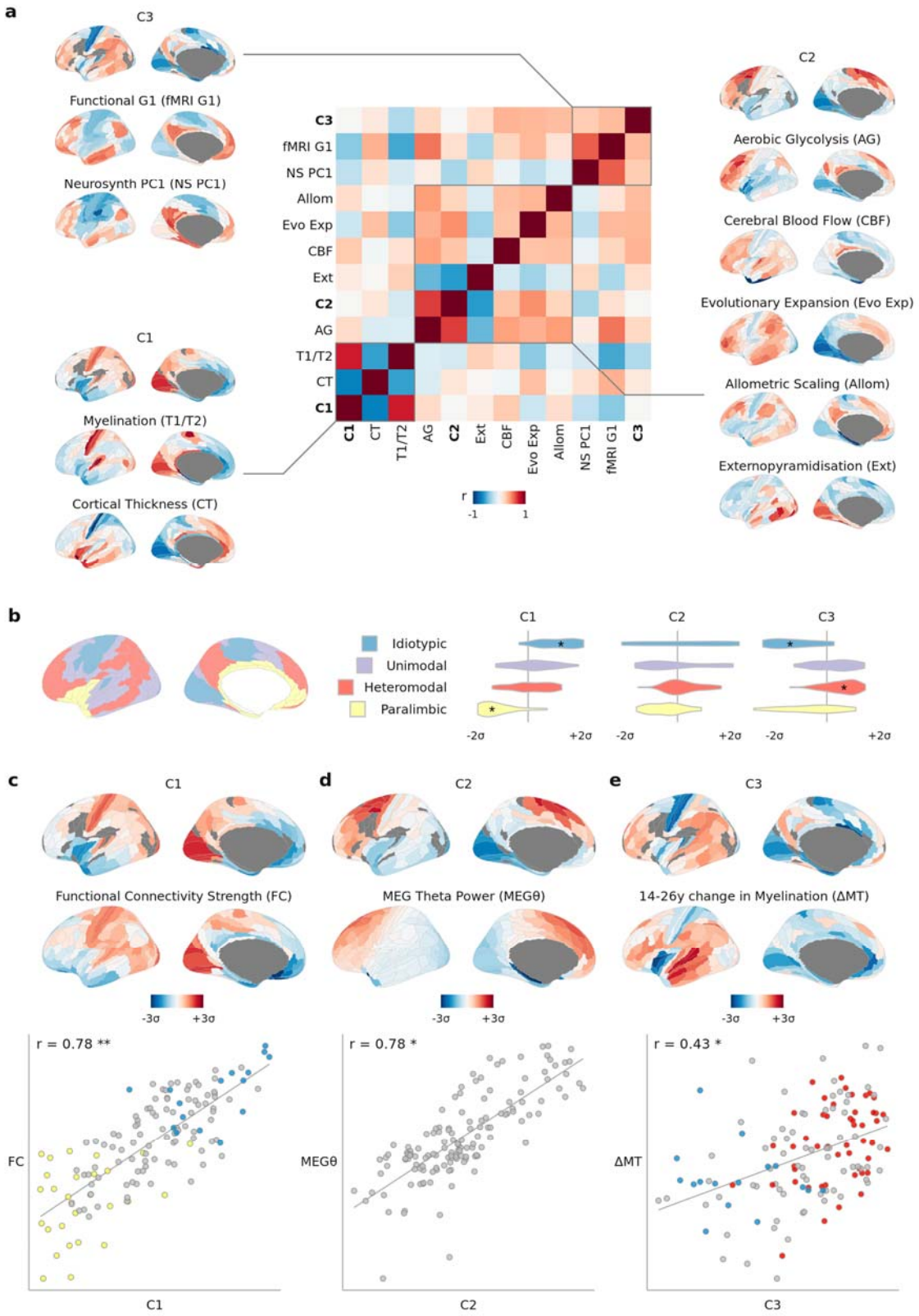

227 ***Figure 2: Neuroimaging and macro-scale maps of brain structure, function, and development were***
228 ***distinctively co-located with three components of cortical gene expression***. ***a***, *Correlation matrix of intrinsic*
229 *transcriptional components C1-C3 together with the nine neuroimaging- and physiologically-derived maps that*
230 *Sydnor et al. combined with C1 to define a 'sensorimotor-association axis' of brain organisation* [10]. *Many of the*
231 *maps were not highly correlated to each other (median |r|=0.31), and data-driven clustering of the matrix*
232 *revealed three distinct clusters around each of the mutually orthogonal transcriptional components C1-C3,*
233 *demonstrating that all three components are relevant for understanding macroscale brain organisation.* ***b***,
234 *Distributions of regional scores of C1-C3 in histologically-defined regions of laminar cytoarchitecture* [52]. *C1*
235 *distinguished idiotypic (p = 0.005) and paralimbic regions (p = 0.002), while C3 distinguished idiotypic (p = 0.002)*
236 *and heteromodal regions (p = 0.01). * indicates FDR-adjusted two-sided p-value < 0.05, where p-value was*
237 *computed by permutation test as the percentile of the mean z-score relative to null spin permutations, with*
238 *adjustment for multiple comparisons across all 12 tests.* ***c***, *Degree of fMRI functional connectivity* [53,54] *was*
239 *significantly aligned to C1 (r = 0.78,* p_{spin} *< 0.001). Blue/yellow highlighted points correspond to*
240 *idiotypic/paralimbic cytoarchitectural regions as in b.* ***d***, *MEG-derived theta power* [55] *was significantly aligned to*
241 *C2 (r = 0.78,* p_{spin} *= 0.002).* ***e***, *Regional change in myelination over adolescence* [56,57] *was significantly aligned to C3*
242 *(r = 0.43,* p_{spin} *= 0.009). Blue/red highlighted points correspond to idiotypic/heteromodal cytoarchitectural regions*
243 *as in b. For panels c-d, *, **, *** respectively indicate FDR-corrected two-sided spin-permutation p-values: 0.05,*
244 *0.01, 0.001, with corrections for multiple comparisons of all maps in panels c-d being compared with all of C1-C3.*
245

246 We also found that the three transcriptional components were associated with a wider range of
247 cellular, functional and developmental phenotypes than the 9 neuroimaging maps above, and that
248 these associations were again distinct for the three components. For example, at cellular scale,
249 histologically-defined regions of laminar cytoarchitectural differentiation [52] were co-located with C1
250 and C3, but not C2 (ANOVA, p < 0.001; **Fig. 2b**). In functional MRI and magnetoencephalography
251 (MEG) data, we found that weighted nodal degree of cortical regions in an fMRI network [53,54] was
252 strongly correlated with C1 (r_{C1} = 0.78, p_{spin} < 0.001, FDR = 5%, **Fig. 2c**) but not C2 or C3 (r_{C2} = -0.01, r_{C3}
253 = 0.00); across all canonical frequency intervals of MEG data [55], an FDR-significant association was
254 observed between theta band (4-7 Hz) oscillations and C2 (r_{C2} = 0.78, p_{spin}=0.002, FDR = 5%, **Fig. 2d**)
255 but not C1 or C3 (r_{C2} = -0.18, r_{C3} = -0.02); see **Extended Data Fig. 5** for other MEG results. And in
256 support of the hypothetical prediction that adult brain transcriptional programmes are
257 neurodevelopmentally relevant, we found that a prior map of adolescent cortical myelination, as
258 measured by change in magnetisation transfer between 14-24 years (ΔMT) [56,57], was significantly co-
259 located with C3 (r_{C3} = 0.43, p_{spin} = 0.009, **Fig. 2e**) but not C1 or C2 (r_{C2} = 0.17, r_{C3} = 0.15).
260

261 ## C1-C3 are distinctly developing intra-cellular programmes

262 We next used two additional RNA-seq datasets to investigate the consistency of AHBA-derived
263 components with gene co-expression in single cells, e.g., neurons or glia, and to explore the
264 developmental phasing of gene transcription programmes represented by C1-C3.
265
266 First, for single-cell RNA-seq data comprising 50,000 nuclei sampled from five cortical regions of three
267 donor brains [58], the total weighted expression of the C1-C3 gene weights in each sample was
268 computed separately for genes positively and negatively weighted in each component (**Methods**). We
269 reasoned that if the components derived from bulk tissue microarray measurements in the AHBA
270 dataset were merely reflective of regional differences in cellular composition, e.g. neuron-glia ratio,
271 then genes weighted positively and negatively on each component should not have anti-correlated
272 expression across cells of the same class. However, we observed that genes weighted positively and
273 negatively on the same component had strongly anti-correlated expression at the single-cell level (**Fig.**
274 **3a**), whereas genes that were positively and negatively weighted on different components were not
275 anti-correlated (**Supplementary Fig. S5**). The anti-correlation of genes positively and negatively
276 weighted on C1 or C2 was stronger within each class of cells than across multiple cell classes; and even
277 stronger when the single-cell data were stratified by sub-classes of cells in specific cortical layers, e.g.,
278 L2 VIP-expressing interneurons (**Fig. 3a inset**). In contrast, for C3 the anti-correlation of positively and
279 negatively weighted genes was stronger across cell classes than within each class, although there was
280 still evidence for significantly coupled expression across cells of the same class or subclass.
281

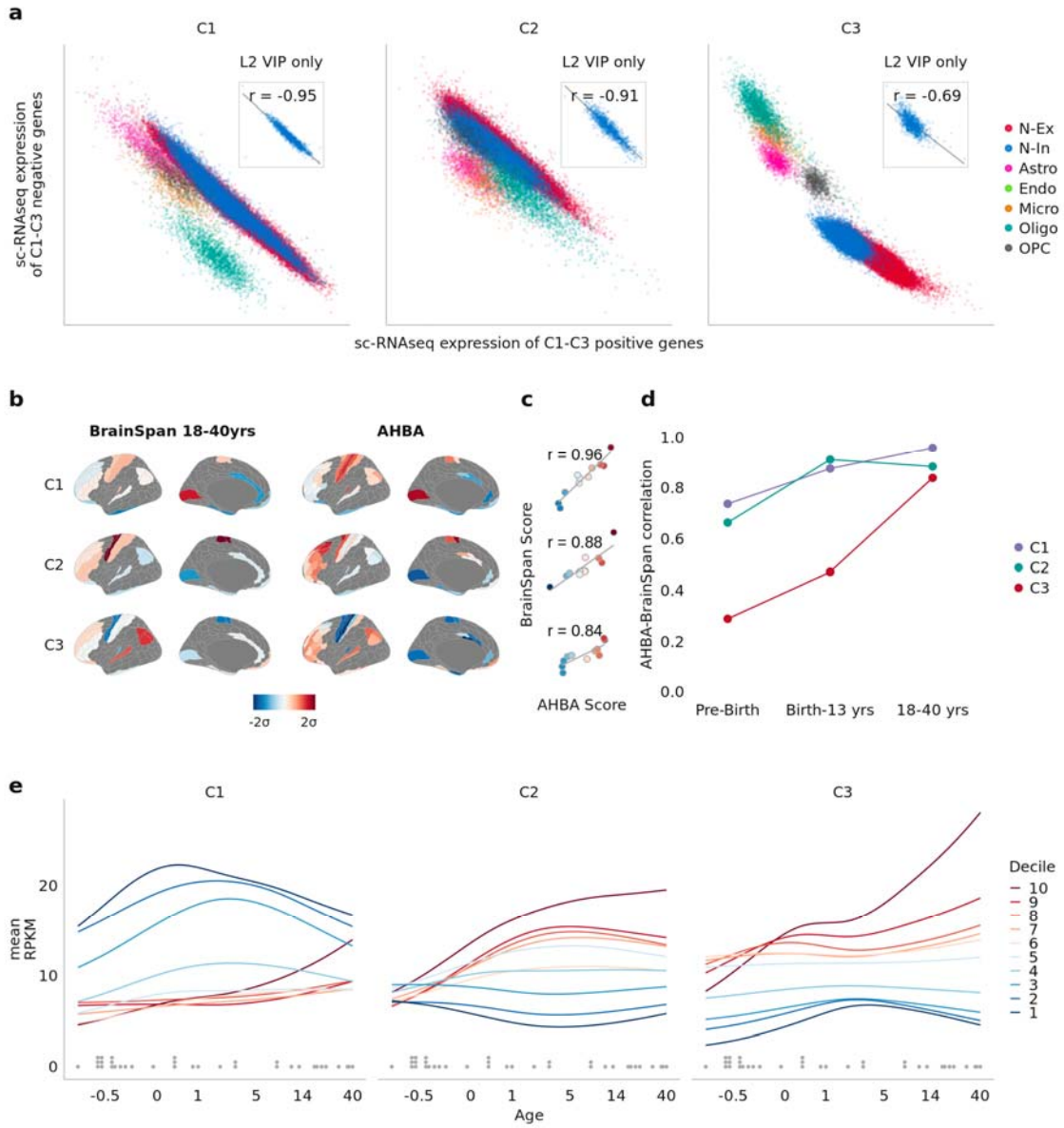

***Figure 3**: Transcriptional components represent intracellular coordination of gene expression programmes with distinct developmental trajectories. **a**, For each of ~50,000 single-cell RNAseq samples, the weighted average expression of the negatively-weighted genes of each AHBA component C1-C3 is plotted against that of the positively-weighted genes (Methods). Samples are coloured by cell-type, demonstrating that genes positively and negatively weighted on C1-C3 have correlated expression within each major class of brain cells: N-Ex, excitatory neurons; N-In, inhibitory neurons; Astro, astrocytes; Endo, endothelial cells; Micro, microglia; Oligo, oligodendrocytes; and OPC, oligodendrocyte precursor cells. Inset, a subset of samples from Layer 2 VIP interneurons, illustrating that C1-C3 weighted genes were transcriptionally coupled even within a fine-grained, homogeneous group of cells. **b**, Cortical maps representing the regional scores of components C1-C3 for each of 11 regions with transcriptional data available in the BrainSpan cohort of adult brains (left) and C1-C3 component scores for the matching subset of regions in the AHBA (right). **c**, Scatter plots of matched regional C1-C3 scores*

from b, demonstrating that the three transcriptional components defined in the AHBA had consistent spatial expression in BrainSpan. ***d****, Correlations between AHBA C1-C3 scores and BrainSpan C1-C3 scores (as in c) for each of 3 age-defined subsets of the BrainSpan dataset. C1 and C2 component scores were strongly correlated between datasets for all age subsets, whereas C3 component scores were strongly correlated between datasets only for the 18-40y subset of BrainSpan. This indicates that C1 and C2 components were expressed in nearly adult form from the earliest measured phases of brain development, whereas C3 was not expressed in adult form until after adolescence.* ***e****, Developmental trajectories of brain gene expression as a function of age (-0.5 to 40 years; x-axis, log scale) were estimated for each gene (Methods) and then averaged within each decile of gene weights for each of C1-C3; fitted lines are colour-coded by decile. Genes weighted positively on C3 were most strongly expressed during adolescence, whereas genes weighted strongly on C1 or C2 were most expressed in the first 5 years of life. Dots above the x-axis represent the post-mortem ages of the donor brains used to compute the curves. RPKM: reads per kilobase million.*

Second, to explore the developmental trajectories of the transcriptional components, we used BrainSpan, an independent dataset where gene expression was measured by RNA-seq of bulk tissue samples from between 4 and 14 cortical regions for each of 35 donor brains ranging in age from -0.5 years (mid-gestation) to 40 postnatal years [6]. We first asked if the gene weights for each of the components derived from the AHBA dataset would exhibit similar spatial patterns in the BrainSpan dataset. We projected the C1-C3 gene weights from the AHBA onto the subset of adult brains (18-40 years, N = 8) in BrainSpan (**Fig. 3b**, **Methods**) and found that the resulting cortical maps of component scores in the BrainSpan data were highly correlated with the corresponding cortical maps derived from the AHBA dataset (r_{C1} = 0.96, r_{C2} = 0.88, r_{C3} = 0.84; **Fig. 1d**). This indicated that the three components defined in the AHBA were generalisable to the adult brains in the BrainSpan dataset (for a full replication of C1-C3 in independent data see **Extended Data Fig. 3**). We then similarly compared the cortical component maps derived from the AHBA dataset to the corresponding maps calculated for subsets of the BrainSpan cohort from two earlier developmental stages (prebirth, N = 20, and birth-13 years, N = 14). We observed that for C1 and C2, AHBA component scores were almost as highly correlated with BrainSpan component scores in foetal (prebirth) and childhood (birth-13 years) brains as in the adult (18-40 years) brains (birth-13 years, r_{C1} = 0.87, r_{C2} = 0.91; prebirth, r_{C1} = 0.74, r_{C2} = 0.66; **Fig. 3d**). However, C3 scores in the AHBA dataset were not so strongly correlated with C3 scores in the foetal and childhood subsets of the BrainSpan dataset (prebirth, r_{C3} = 0.29; birth-13 years, r_{C3} = 0.47). These results suggested that C3 may only emerge developmentally during adolescence, whereas the C1 and C2 have nearly-adult expression from the first years of life.

We tested this hypothesis by further analysis of the BrainSpan dataset, modelling the non-linear developmental trajectories of each gene over the age range -0.5 to 40 years (**Methods**) and then

330 averaging trajectories over all genes in each decile of the distributions of gene weights on each of the
331 three components. We found that genes in the top few deciles of C3 gene weights became more
332 strongly expressed during and after adolescence, whereas genes in the top few (C2) or bottom few
333 (C1) deciles of gene weights on the other two components were most strongly expressed in the first 5
334 years of life and then declined or plateaued during adolescence and early adult life (**Fig. 3e**). These
335 results confirmed that components C1-C3 have distinct neurodevelopmental trajectories, with genes
336 positively weighted on C3 becoming strongly expressed after the first postnatal decade.
337

338 Autism and schizophrenia have specific links to C1/C2 and C3

339 Finally, we explored the clinical relevance of C1-C3 by analysis of prior neuroimaging, differential gene
340 expression, and GWAS associations for autism spectrum disorder (ASD), major depressive disorder
341 (MDD), and schizophrenia.
342
343 First, we leveraged the BrainChart neuroimaging dataset of >125,000 MRI scans [59], in which atypical
344 deviation of regional cortical volumes in psychiatric cases was quantified by centile scores relative to
345 the median growth trajectories of normative brain development over the life-cycle (**Fig. 4a**). Using the
346 Desikan-Killiany parcellation of 34 cortical regions necessitated by alignment with this dataset
347 (**Methods**), we found that cortical shrinkage in ASD was significantly associated with both C1 and C2
348 (r_{C1} = 0.49, p_{spin} = 0.0002, FDR < 5%; r_{C2} = -0.28, p_{spin} = 0.0006, FDR < 5%), while shrinkage in
349 schizophrenia was specifically associated with C3 (r_{C3} = 0.43, p_{spin} = 0.008, FDR < 5%) (**Fig. 4b**).
350
351 Second, we compiled consensus lists of differentially expressed genes (DEGs) from RNA-seq
352 measurements of dorsolateral prefrontal cortex tissue in independent studies of ASD [36,64,65], MDD [66],
353 and schizophrenia [65,67–70] (**Methods**). We found that genes differentially expressed in ASD were
354 specifically enriched in both C1 and C2 (but not C3); whereas genes differentially expressed in
355 schizophrenia were enriched in C3 (but not C1 or C2); and genes differentially enriched in MDD were
356 enriched only in C1 (**Fig. 4b**). Corroborating the enrichments of ASD DEGs, case-control differences in
357 expression at 11 cortical regions for ASD cases compared to healthy controls showed the positively
358 weighted genes on C1 and C2 were significantly less strongly expressed in ASD cases than in controls
359 (**Extended Data Fig. 3**).
360

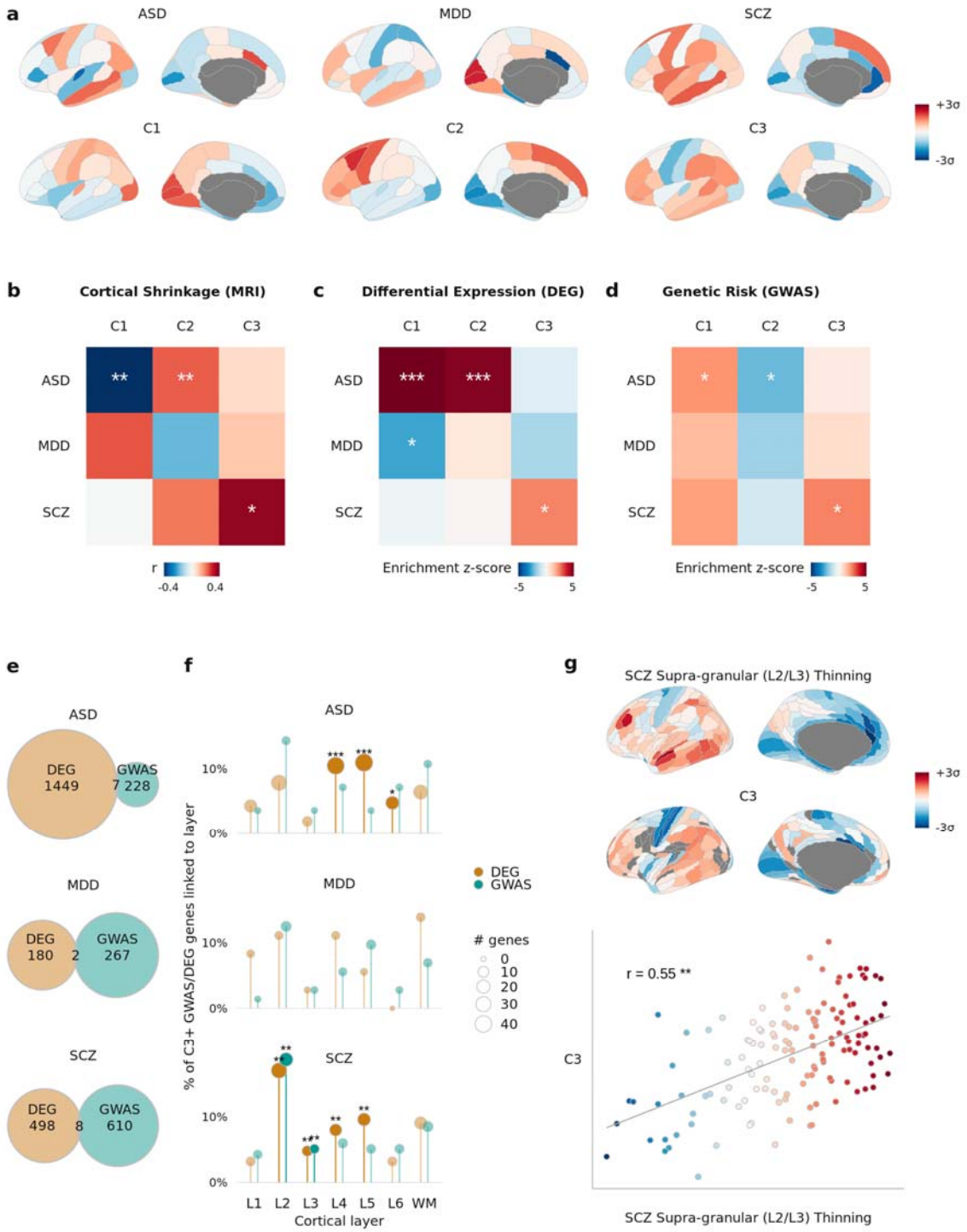

***Figure 4**: **Genetics, transcriptomics, and neuroimaging of autism and schizophrenia were consistently and specifically linked to normative transcriptional programmes. a**, First row: cortical volume shrinkage in autism spectrum disorder (ASD), major depressive disorder (MDD), and schizophrenia (SCZ) cases. Red indicates greater shrinkage, computed as z-scores of centiles from normative modelling of >125,000 MRI scans. Second row: AHBA components projected into the same Desikan-Killiany parcellation. **b**, Spatial correlations between volume changes and AHBA components, C1-C3. Significance tested by spatially autocorrelated spin permutations, and*

368 *corrected for multiple comparisons: *, **, *** respectively indicate FDR-adjusted two-sided p-values: 0.05, 0.01,*
369 *0.001.* ***c****, Enrichments in C1-C3 for consensus lists of differentially expressed genes (DEGs) in postmortem brain*
370 *tissue of donors with ASD, MDD, and SCZ compared to healthy controls (Methods). Significance assessed as*
371 *percentile of mean weight of DEGs in each component relative to randomly permuted gene weights, and*
372 *corrected for multiple comparisons: *, **, *** respectively indicate FDR-adjusted two-sided p-values: 0.05, 0.01,*
373 *0.001.* ***d****, Enrichment in C1-C3 for GWAS risk genes for ASD[60], MDD[61], and SCZ[62], tested for significance as in c,*
374 *demonstrating alignment with both spatial associations to volume changes and enrichments for DEGs.* ***e,*** *Venn*
375 *diagrams showing the lack of overlap of DEGs and GWAS risk genes reported by the primary studies summarised*
376 *in panels c and d.* ***f****, DEGs and GWAS risk genes for each disorder were filtered for only C3-positive genes, then*
377 *tested for enrichment with marker genes for each cortical layer [38]. Significance was tested by one-sided Fisher's*
378 *exact test and corrected for multiple comparisons across all 42 tests. C3-positive DEGs and GWAS genes for SCZ*
379 *(but not ASD or MDD) were both enriched for L2 and L3 marker genes, despite the DEGs and GWAS gene sets*
380 *having nearly no overlap for each disorder (see* ***Extended Data Fig. 6*** *for more detail).* ***g,*** *Convergent with L2/L3*
381 *enrichment in the C3-positive schizophrenia-associated DEGs and GWAS genes, a cortical map of supragranular-*
382 *specific cortical thinning in schizophrenia [63] was significantly and specifically co-located with C3 (r = 0.55, two-*
383 *sided spin-permutation p-value = 0.002); each point is a region, color represents C3 score.*
384
385 Third, using data from the most recent GWAS studies of ASD [60], MDD [61], and schizophrenia [62], we
386 found that genetic variants significantly associated with ASD were enriched in both C1 and C2 (but not
387 C3); whereas genes associated with schizophrenia were enriched in C3 (but not C1 or C2) (**Fig. 4d**).
388 Genes associated with MDD were not significantly enriched in any transcriptional component. These
389 associations were replicated when using alternative methods (MAGMA [71] and H-MAGMA [72]) to test
390 the association between GWAS-derived p-values for the association of each gene with ASD, MDD or
391 schizophrenia and the C1-C3 gene weights without requiring an explicit prioritisation of GWAS-
392 associated genes (**Supplementary Fig. S6**). This pattern of results for autism and schizophrenia GWAS
393 associations evidently mirrored the pattern of prior results from analysis of case-control neuroimaging
394 (**Fig. 4b**) and differential gene expression studies (**Fig. 4c**), with ASD consistently linked to components
395 C1 and C2, and schizophrenia consistently linked to C3.
396
397 Notably, this consistency of association between disorders and specific transcriptional components
398 was observed despite minimal overlap between the DEGs and GWAS risk genes identified as
399 significant by the primary studies of each disorder [73] (**Fig. 4e**). However, motivated by the association
400 of C3 with regions of greatest laminar differentiation (**Fig. 2b**), we found that the subsets of the
401 schizophrenia-associated DEG and GWAS gene sets that were positively-weighted on C3 were both
402 significantly enriched for marker genes of layers L2 and L3 (**Fig. 4g; Extended Data Fig. 6**). These
403 shared laminar associations between the non-overlapping DEG and GWAS gene sets were only present

404 when subsetting to C3-positive genes, and were specific to schizophrenia (i.e. C3-positive subsets of
405 ASD and MDD genes did not show the same L2/L3 enrichments). Convergent with C3 revealing an
406 L2/L3 association in schizophrenia-associated genes from DEG and GWAS, we found that the cortical
407 map of C3 was significantly co-located with an MRI-derived map of specifically supragranular, L2/L3
408 predominant thinning in schizophrenia [63] (r_{C3} = 0.55, p_{spin} = 0.002, FDR < 1%, **Fig. 4g**).
409
410
411
412

413 Discussion

414 Our results offer a new perspective on how the brain's macroscale organisation develops from the
415 microscale transcription of the human genome. Through optimized processing of the AHBA and
416 replication in PsychENCODE, we have shown that the transcriptional architecture of the human cortex
417 comprises at least three generalisable components of coordinated gene expression. The two higher-
418 order components (C2 and C3) had not previously been robustly demonstrated, although the initial
419 AHBA paper identified similar components to C1 and C2 by applying PCA to one of the six AHBA brains
420 and filtering for only 1000 genes [2] (**Supplementary Fig. S1**). Here we derive C2 and C3 from all six
421 AHBA brains and show they each represent the coordinated expression of hundreds of genes
422 (**Supplementary Fig. S2**). Broadly, the C2 genes were enriched for "metabolic" and "epigenetic"
423 processes, while the C3 genes were enriched for "synaptic" and "immune" processes (**Fig. 1c**). Both
424 higher-order components were significantly enriched for genes associated with intelligence and
425 educational attainment (**Fig. 1f-g**), indicating their relevance to the brain's ultimate purpose of
426 generating adaptive behaviour. The brain maps corresponding to each of the components were also
427 distinctively co-located with multiple neuroimaging or other macroscale brain phenotypes (**Fig. 2**).
428 These co-locations were often convergent with the gene enrichment results, triangulating evidence
429 for C2 as a metabolically specialised component and for C3 as a component specialised for synaptic
430 and immune processes underpinning adolescent plasticity; see **Table 1**. Together, these convergent
431 results expand on the proposal of a single "sensorimotor-association axis" [10,74] by demonstrating that
432 macro-scale brain organisation emerges from multiple biologically-relevant transcriptional
433 components.
434
435
436
437

438

		C1: Neuronal hierarchy	C2: Cognitive metabolism	C3: Adolescent plasticity
Normative	***Biological processes*** (Fig. 1c)	*Most genes are aligned, especially PVALB, SST*	*Metabolism Epigenetics*	*Synaptic plasticity Learning/memory Immunity*
	Architectonics (Fig. 1d)	*L4 L1, L2, L6*	*L4, L5, L6 L2*	*L2, L3, L4, L5, L6 L1, WM*
	Cell types (Fig. 1e)	*Oligodendrocytes Astrocytes*	*Synapses, Endothelial cells*	*Synapses, Neurons Oligodendrocytes, Microglia*
	GWAS (Fig. 1f-g)	*Educational attainment*	*Intelligence/cognition Educational attainment*	*Intelligence/cognition Educational attainment*
	Imaging (Fig. 2)	fMRI degree T1w/T2w Cortical thickness	MEG theta power Aerobic glycolysis	Adolescent change in myelination
	Development (Fig. 3b-c)	Prenatal, greatest expression at birth	Prenatal, greatest expression in first decade	Adolescence, greatest expression in adulthood
Atypical	**Imaging** (Fig. 4a-b, g)	ASD volume shrinkage	ASD volume shrinkage	SCZ volume shrinkage and L2, L3-specific thinning
	RNA-seq of brain tissue (Fig. 4c,f)	ASD DEGs	ASD DEGs	SCZ DEGs, with L2, L3 enrichment
	GWAS (Fig. 4d,f)	*ASD risk genes*	*ASD risk genes*	*SCZ risk genes, with L2, L3 enrichment*

439 ***Table 1: Summary of convergent results on the biological and clinical relevance of three human brain***
440 ***transcriptional programmes.*** *Each of three components of normative human brain gene expression (C1, C2, C3;*
441 *table columns) was biologically validated by testing for enrichment of gene weights on each component, and for*
442 *co-location of regional component scores with neuroimaging or other macro-scale brain phenotypes, in healthy*
443 *brain samples (normative) and in studies of neurodevelopmental disorders (atypical). Each row summarises*
444 *results for a distinct gene enrichment analysis (italicised) or spatial co-location analysis (plain font). Based on*
445 *prior knowledge that theta oscillations are linked to intelligence and cognition* [75] *as well as to glucose*
446 *metabolism* [76]*, the spatial alignments between C2 and maps of MEG theta power (**Fig. 2d**) and aerobic glycolysis*
447 *(**Fig. 2a**) were convergent with the enrichment of C2 for genes linked to cognitive capacity (**Fig. 1f-g**) and*
448 *metabolism (**Fig. 1c**). Similarly, prior knowledge implicates microglia and oligodendrocytes in the immune-*
449 *mediated synaptic pruning and myelination that over adolescence gives rise to adult cognitive capacity* [77,78]*, such*

450 *that the spatial alignment between C3 and the map of adolescent myelination (**Fig. 2d**) was convergent with the*
451 *enrichments of C3 for genes related to immunity, synaptic development, and learning (**Fig. 1c**); oligodendrocytes,*
452 *microglia, and synapses (**Fig. 1e**); and cognitive capacity (**Fig. 1f-g**), among which one GWAS study explicitly*
453 *linked intelligence to myelination [41].*
454
455 The discovery of these biologically-relevant, higher-order transcriptional components in the AHBA
456 dataset raised further questions: i) do the components reflect coordinated gene expression within
457 cells, or only variation in cell composition; ii) when do the components emerge during brain
458 development; and (iii) how do they intersect with neurodevelopmental disorders? We addressed
459 these questions using additional RNA-seq datasets (**Supplementary Table S5**). First, we found that
460 genes positively or negatively weighted on the components derived from the AHBA bulk tissue
461 samples had consistently coupled co-expression across RNA-seq measurements in single cells, e.g.
462 individual neurons and glia (**Fig. 3a**). This indicated that C1-C3 represent transcriptional programmes
463 coordinated at the intracellular level, not merely regional variation in the proportion of different cell
464 types. Second, we found that C1-C3 have differentially phased developmental trajectories of
465 expression, e.g. that the positive pole of C3 becomes strongly expressed only during adolescence,
466 convergent with its spatial co-location with a map of adolescent cortical myelination (**Fig. 3b-c**).
467 Finally, we established that these transcriptional programmes are not only critical for healthy brain
468 development but, as might be expected, are also implicated in the pathogenesis of
469 neurodevelopmental disorders (**Fig. 4**).
470
471 The pattern of results for disorders was strikingly convergent across multiple data modalities: C1 and
472 C2 were both enriched for genes implicated by both GWAS and DEG data on ASD, whereas C3 was
473 specifically enriched for genes implicated by both GWAS and DEG data on schizophrenia (**Table 1**). We
474 observed a similar pattern of significant co-location between C1-C3 maps and MRI phenotypes:
475 developmentally normalised scores on reduced cortical volume in ASD were correlated with maps of
476 C1 and C2, and for schizophrenia with the map of C3 (**Fig. 4a-b**). In contrast, there was no evidence for
477 enrichment of C1-C3 by genes associated with risk of Alzheimer's disease [79] (**Supplementary Fig. S6**).
478 An intuitive generalisation of these results is that the developmental processes which give rise to
479 these three components of gene expression in the healthy adult brain are pathogenically more
480 relevant for neurodevelopmental disorders than for neurodegenerative disease.
481
482 Overall, our results were strongly supportive of the motivating hypothesis that the transcriptional
483 architecture of the human cortex represents developmental programmes crucial both to the brain's
484 healthy organisation and to the emergence of neurodevelopmental disorders. For example, when

interpreting C3 as a transcriptional programme mediating adolescent plasticity (**Table 1**), our finding that C3 represents coupled transcription of synapse- and immune-related genes within cells (**Fig. 3a**) is consistent with prior work indicating that the neuronal expression of immune-related, typically glial genes can play a mechanistic role in synaptic pruning [80]; and, vice-versa, that neuronal genes associated with synapse and circuit development can also be expressed in glial cells [81]. While atypical synaptic pruning has long been hypothesised to be a mechanistic cause of schizophrenia [82–84], prior results on the biology of schizophrenia have shown limited consistency, both between the primary data modalities of GWAS, post-mortem expression, and neuroimaging [85,86], and even between DEG studies [73]. Here, we demonstrate that the C3 transcriptional programme offers a unifying link between these disparate prior results. When parsed by the C3 positive genes, the otherwise non-overlapping GWAS and DEG gene-sets for schizophrenia display a shared enrichment for supra-granular marker genes (**Fig. 4e-f**), and, convergently, C3 was spatially associated with supra-granular-specific thinning in schizophrenia (**Fig. 4g**). Supra-granular layers have dense cortico-cortical connections and are expanded in humans relative to other species [87–89], mature latest in development [90], have been linked to intelligence [91], and have previously been linked to schizophrenia [92–94]. This triangulation of evidence strongly suggests that the third component of the brain's gene expression architecture represents the transcriptional programme coordinating the normative, neuro-immune processes of synaptic pruning and myelination in adolescence [56], such that atypical expression of C3 genes due to schizophrenia genetic risk variants can result in atypical development of supra-granular cortical connectivity leading to the clinical emergence of schizophrenia.

Clearly there are limits to what can be learnt from RNA measurements of bulk tissue samples from six healthy adult brains. Here, we explicitly identified the limits of the AHBA dataset by optimizing data processing against an unbiased measure of generalisability, *g*, which yielded three components. The architecture of human brain gene expression likely involves more than three components; however, our analysis suggests that their discovery will rely on additional high-granularity transcriptional data. In particular, gene expression varies with sex, age, genetics, and environment [95], so we expect that future data will reveal additional components that are more individually variable and demographically diverse than the three we have characterised here. Meanwhile, the code and data that supplement our results can help future research to leverage our work with the unique AHBA resource.

Extended Data Figures

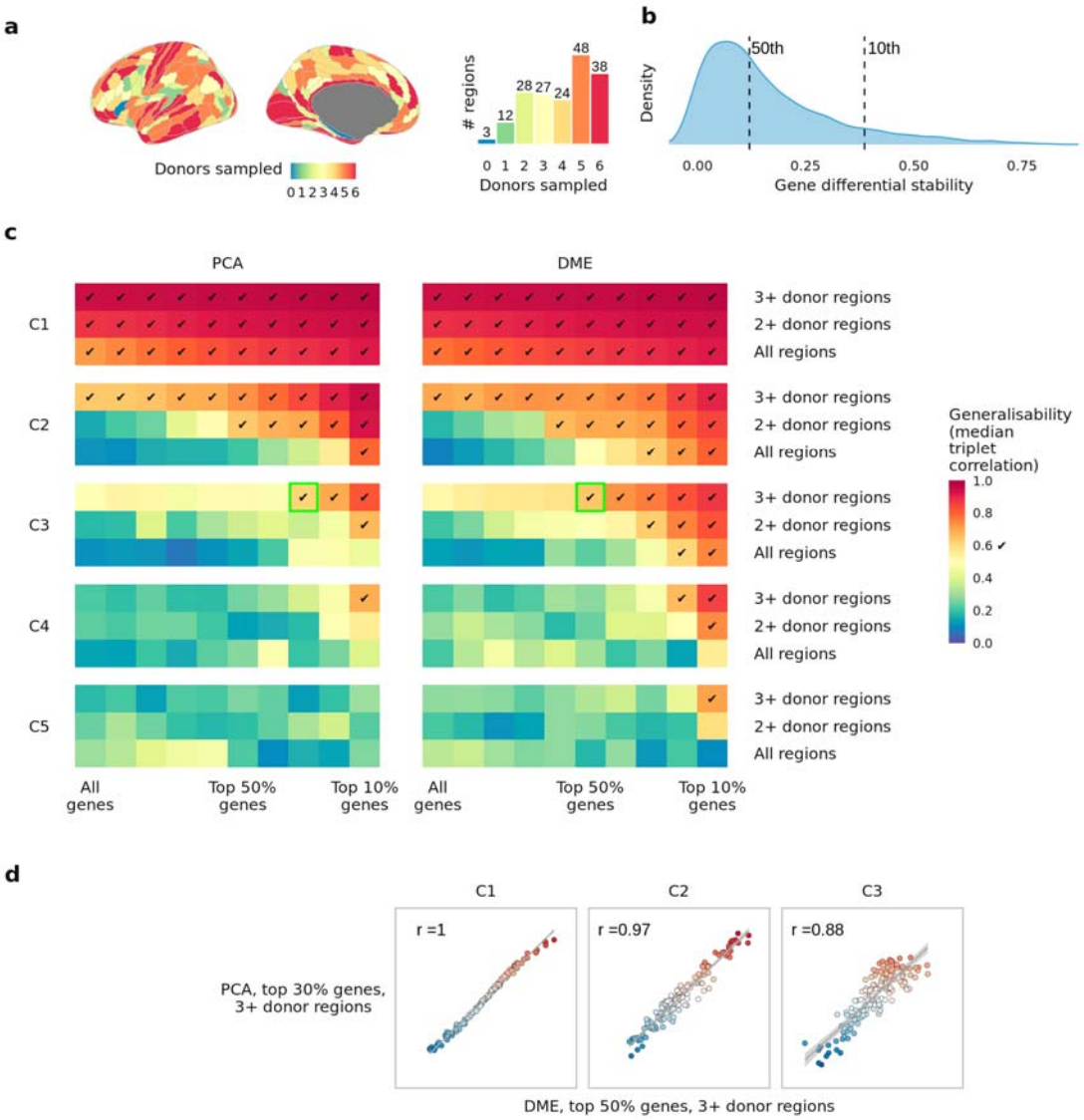

Extended Data Fig. 1: Optimised processing of the AHBA identified three generalisable components. ***a****, In the HCP-MMP parcellation, 43/180 regions are matched to samples representing less than 3 of the 6 AHBA donors.* ***b****, Distribution of differential stability of genes measured in the AHBA dataset processed in the HCP-MMP parcellation.* ***c****, Generalisability of first five components of the AHBA dataset computed with either principal components analysis (PCA) or diffusion map embedding (DME). Color represents generalisability* g*, defined as the median absolute correlation between matched components computed across all 10 disjoint triplet pairs (Methods); x-axis represents variation in the proportion of genes filtered out by differential stability prior to PCA/DME; y-axis represents variation in which regions are filtered out prior to PCA/DME. Tick mark indicates parameter combinations that exceed generalisability g > 0.6. Green highlights for C3 indicate the best parameter option with PCA and DME respectively, showing that switching to DME achieves similar generalisability while retaining more genes.* ***d****, Scatter plots of regional scores for AHBA components computed using the best PCA/DME options, demonstrating that PCA and DME derive spatially equivalent components.*

533

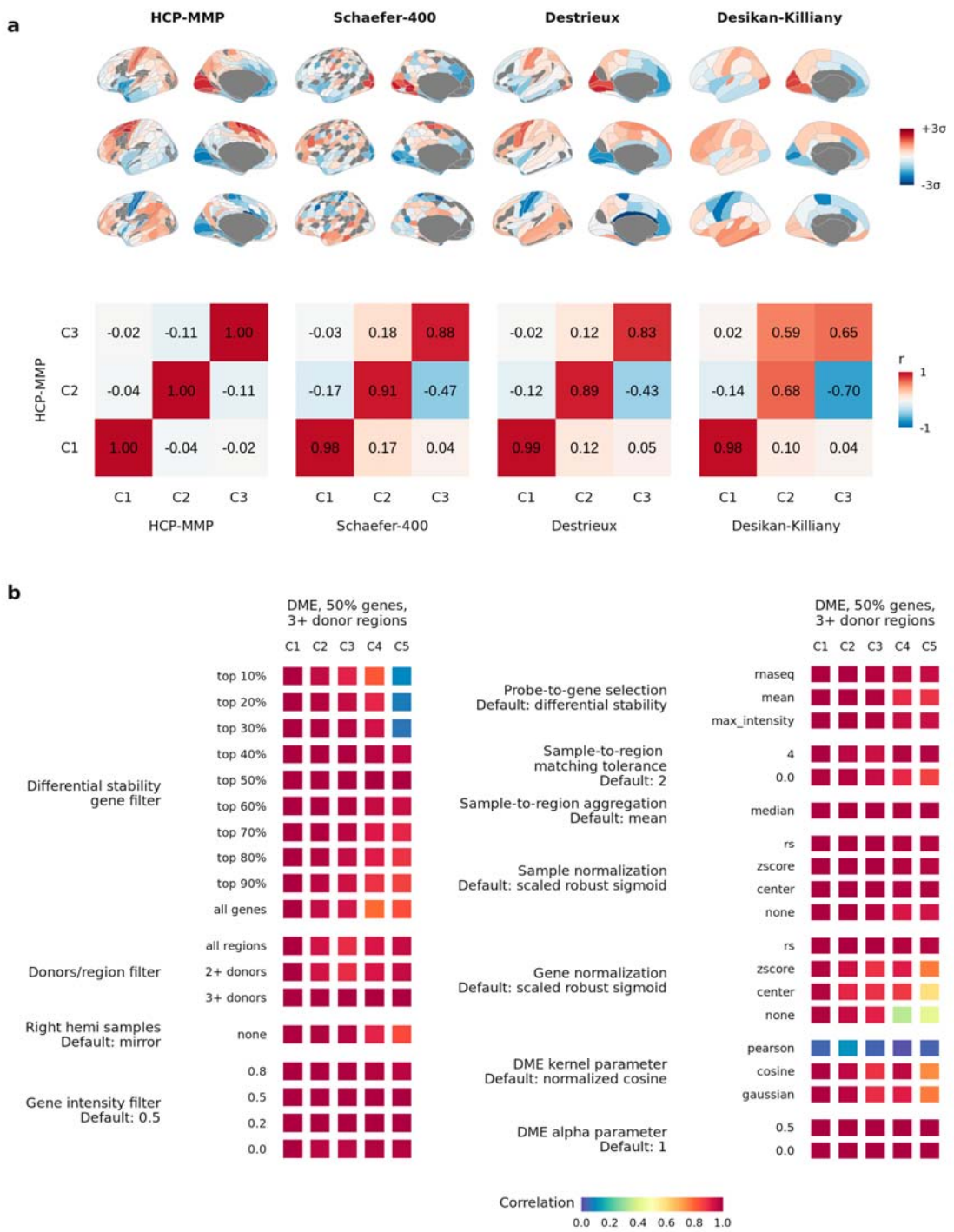

534

535 ***Extended Data Fig. 2: Transcriptional components were robust to parcellation and processing.*** *Transcriptional*
536 *components were computed in four different parcellation templates (Methods). For each parcellation, the gene*
537 *weights for the first three components were correlated with the weights obtained from the HCP-MMP*
538 *parcellation used throughout. Gene weights were highly consistent, although in the less-granular (34-*
539 *regions/hemisphere) Desikan-Killiany parcellation, C2 and C3 were less well aligned to the other parcellations.* ***b****,*

A wide range of parameters for processing the AHBA data were varied, and the resulting component region scores were correlated with the components obtained from the optimised parameters. For nearly all variations in parameters, highly consistent components were obtained, demonstrating the robustness of C1-C3.

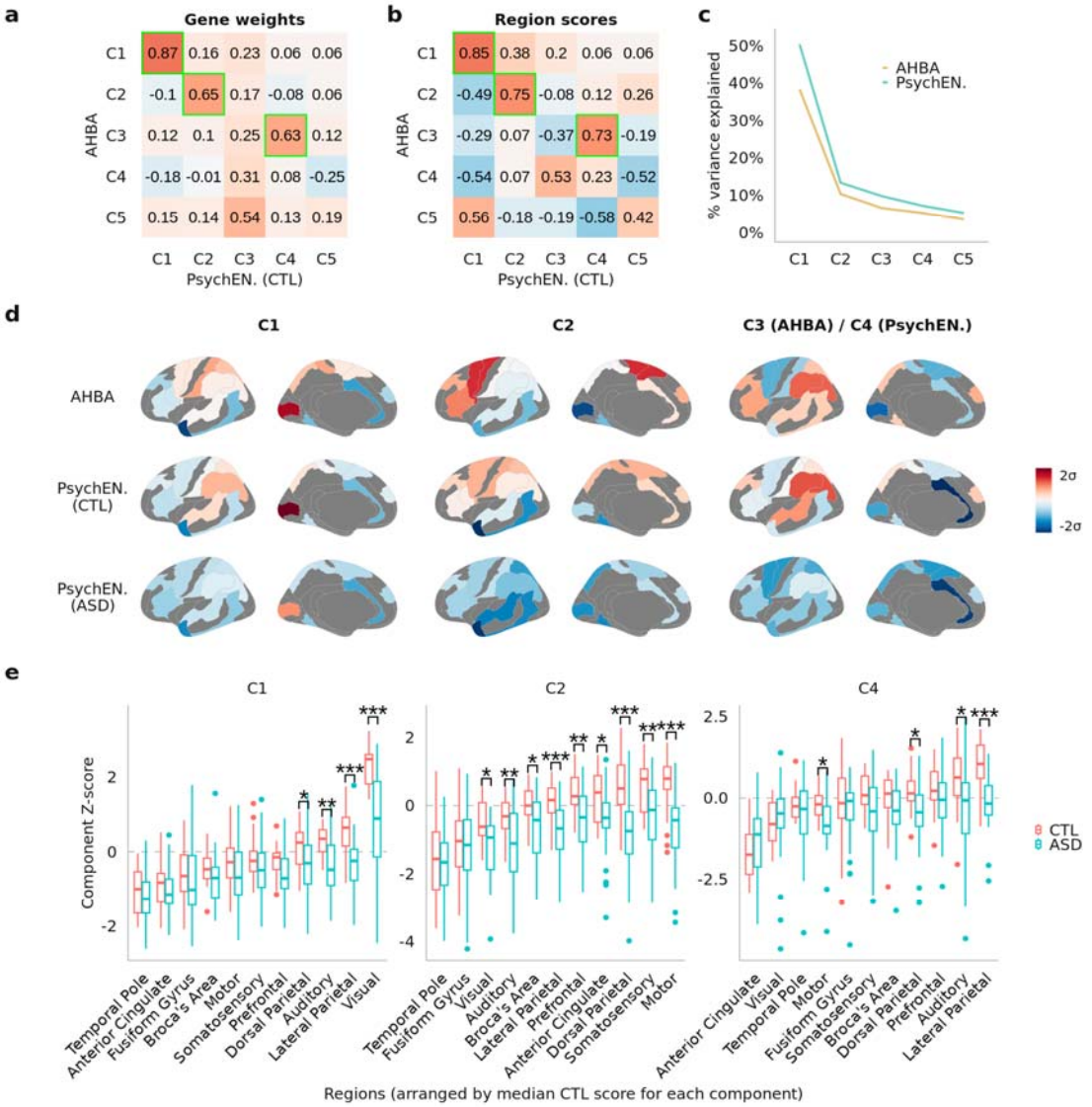

Extended Data Figure 3: AHBA transcriptional components were reproducible in independent PsychENCODE control data, with differential spatial expression in autism. a*, Gene weights from dimension reduction applied to group-averaged bulk RNA-seq measurements from 11 cortical regions in N = 54 healthy control brains from the PsychENCODE dataset [36] were correlated with gene weights from the components of the AHBA (derived by DME in the 180-region HCP-MMP parcellation), showing that the genetic profiles of AHBA C1, C2, and C3 were reproduced by PsychENCODE C1, C2, and C4, respectively (highlighted in green).* ***b****, Regional scores of PsychENCODE C1, C2 and C4 were also correlated with region scores of AHBA C1, C2 and C3, showing that the matching genetic profiles correspond to matching spatial expression patterns.* ***c****, Variance explained by the first five components of each dataset, showing that AHBA C3 and PsychENCODE C4 account for similar proportions of*

variance (6.5% and 7.1%, respectively). ***d****, 1st row: Cortical maps of AHBA C1-C3 in the same 11 regions sampled in the PsychENCODE data. 2nd row: Cortical maps of PsychENCODE C1, C2, and C4 demonstrating their spatial similarity to AHBA C1-C3. 3rd row: Gene weights from the PsychENCODE healthy control data were projected onto transcriptional data of cases with autism spectrum disorder (ASD; N = 58) from the same dataset, demonstrating lower regional expression at the positive (red) pole of each component in the ASD cases compared to healthy controls.* ***e****, Distributions of regional scores for C1, C2 and C4, computed on group-average healthy controls as in a-d and projected to individual donor brains in the PsychENCODE dataset, demonstrating significant case-control differential expression for regions at the positive poles of C1-C3. T-tests of case-control differences were corrected for multiple comparisons across all 33 tests; boxplots represent the median, first, and third quartiles with whiskers showing 1.5 * inter-quartile range; *, **, *** indicate FDR-corrected two-sided p-value < 0.05, 0.01, 0.001 respectively. Region names refer to the sampled Brodmann Areas (BA)* [36]*: Visual = BA17, Temporal Pole = BA38, Somatosensory = BA3-1-2-5, Motor = BA4-6, Anterior Cingulate = BA24, Prefrontal = BA9, Broca's Area = BA44-45, Fusiform Gyrus = BA20-37, Auditory = BA41-42-22, Lateral Parietal = BA39-40, Dorsal Parietal = BA7.*

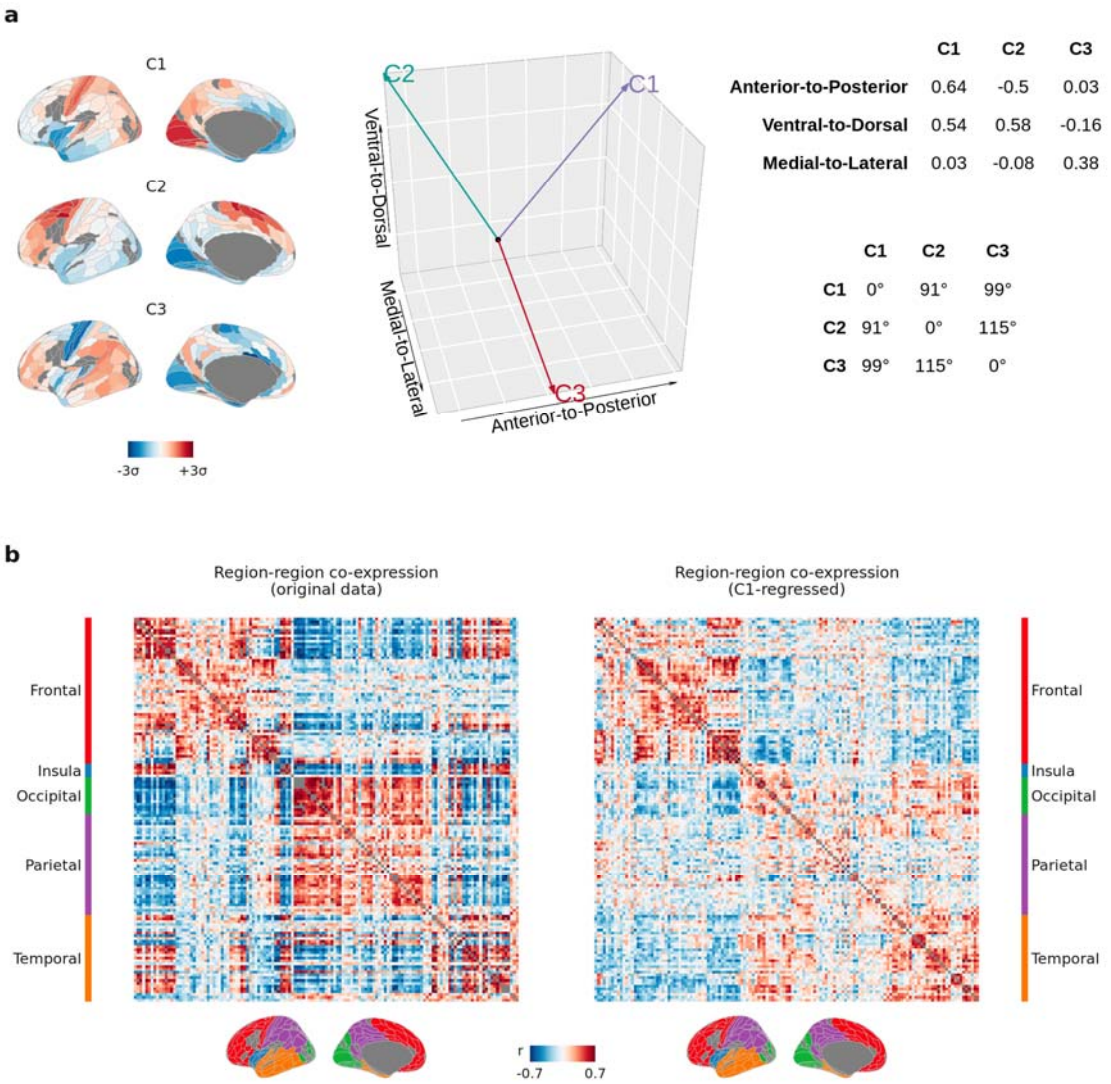

	C1	C2	C3
Anterior-to-Posterior	0.64	-0.5	0.03
Ventral-to-Dorsal	0.54	0.58	-0.16
Medial-to-Lateral	0.03	-0.08	0.38

	C1	C2	C3
C1	0°	91°	99°
C2	91°	0°	115°
C3	99°	115°	0°

Extended Data Figure 4: Higher-order components of cortical gene expression reflect anatomically relevant co-expression structure. a, *C1-C3 were orthogonally aligned in anatomical space, as computed by the Pearson's correlations of the regional scores with the XYZ coordinates of the region centroids: C1 and C2 were both aligned with the anterior-to-posterior (y) and ventral-to-dorsal (z) plane, but with opposite signs along the anterior-to-posterior axis, while only C3 was aligned to the medial-lateral (x) axis. The middle panel represents these alignments as vectors in 3D space. The right-hand upper table shows the correlations of C1-C3 with each anatomical axis, and the lower table shows the angle in degrees between the vectors, showing that C1-C3 are orthogonal.* ***b****, Co-expression matrices computed by Pearson's correlations of gene expression between brain regions, computed with and without regressing out the first component C1, and annotated by the major cortical lobes as defined in the HCP-MMP parcellation [32]. This further demonstrates that the gene co-expression structure captured by C2 and C3 (i.e., the residual variation beyond C1) is anatomically relevant.*

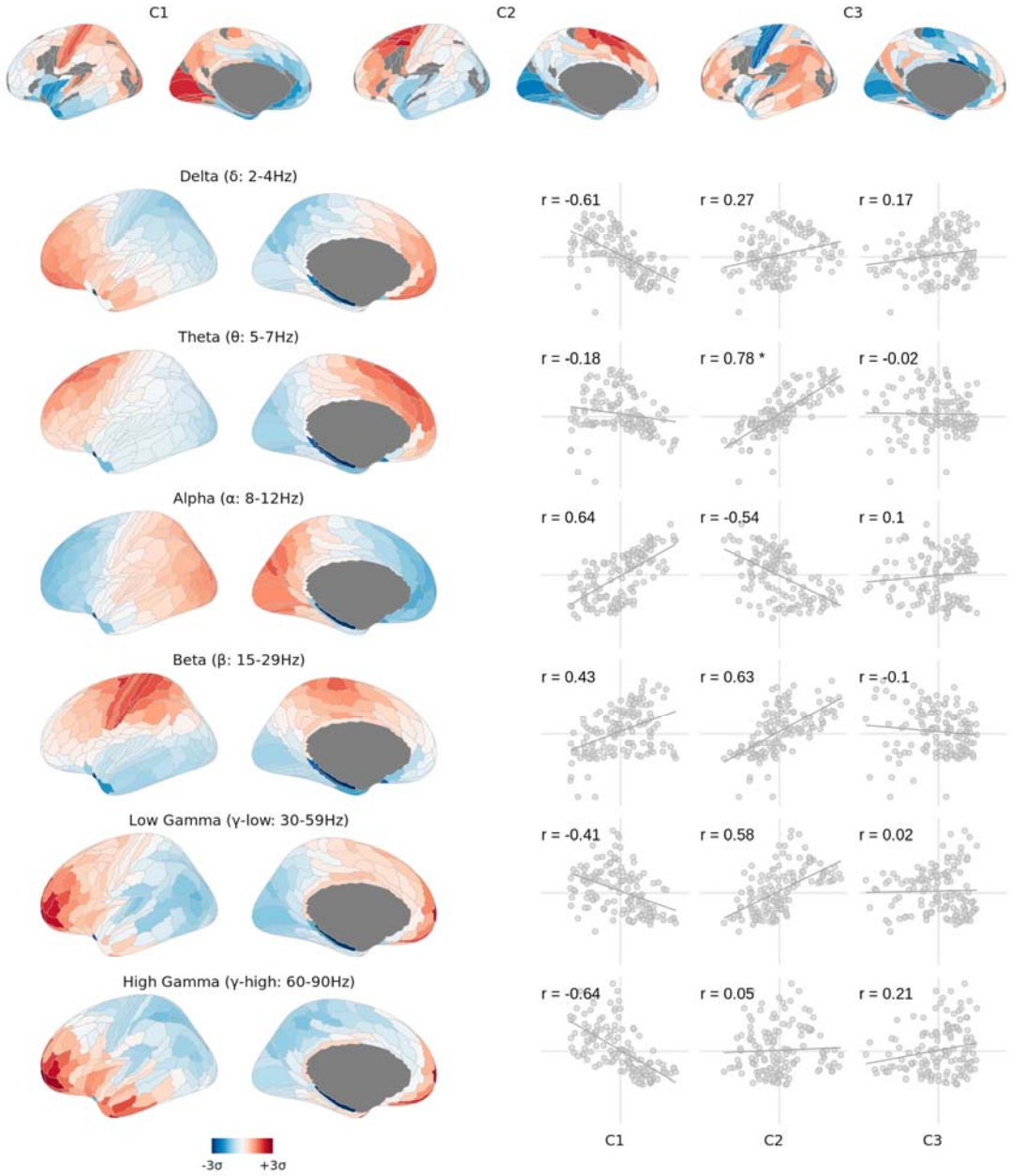

Extended Data Figure 5: Transcriptional components were distinctively associated with the regional power of canonical brain oscillation frequencies. *Several MEG power bands [55] were highly correlated (|r|>0.6) with C1 (delta, alpha, high-gamma) and C2 (beta, theta), although only the theta association to C2 survived FDR correction of the spin-test p-values (r=0.78, FDR_{spin}=0.05). No MEG band was aligned with C3.*

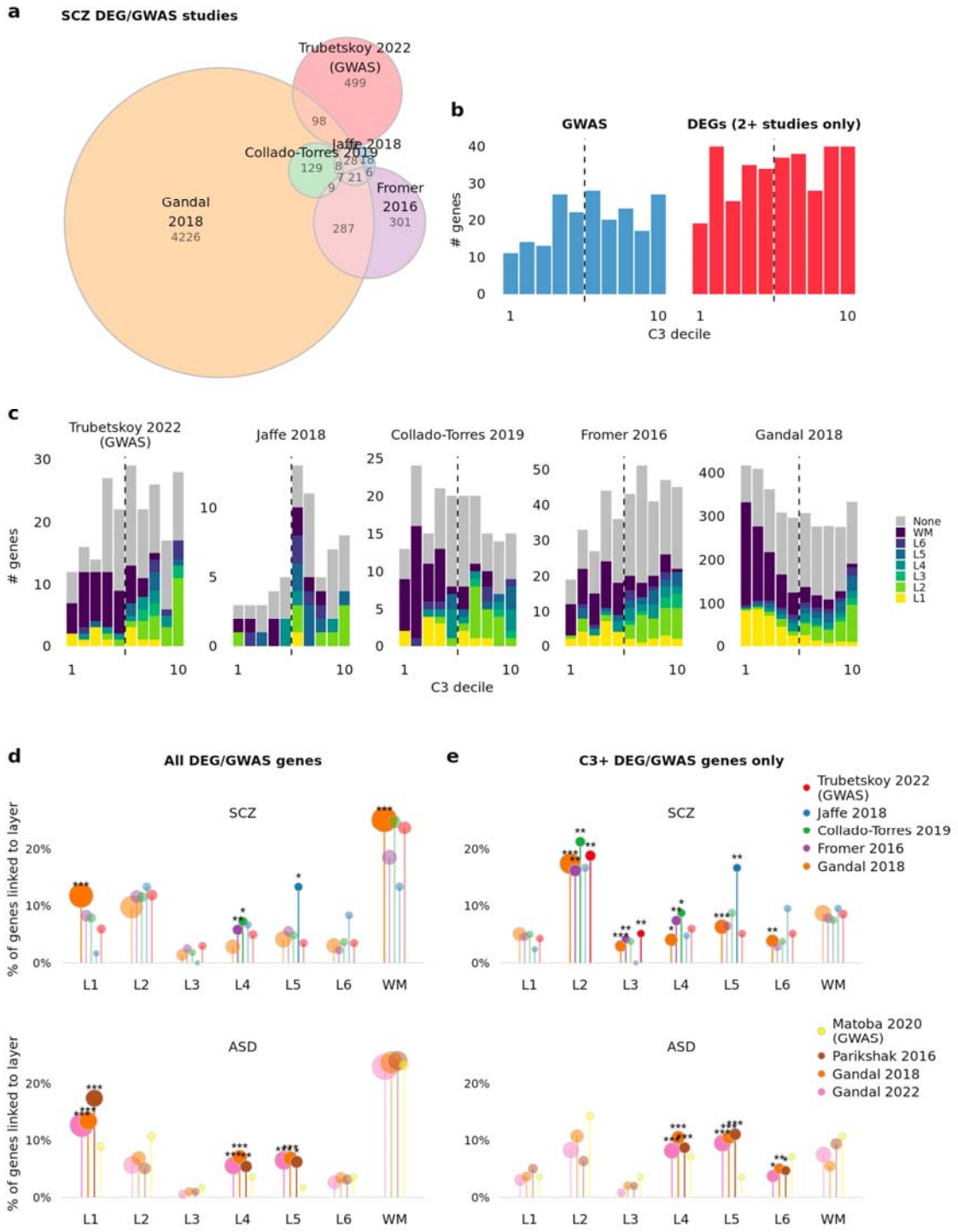

Extended Data Figure 6: C3 reveals shared biology across inconsistent postmortem brain RNA-seq studies of differentially expressed genes (DEGs) in schizophrenia. a*, Euler diagram demonstrating the relative lack of overlap of genes linked to schizophrenia in four independent RNA-seq postmortem brain studies, as well as the latest GWAS study.* ***b****, Histogram of the schizophrenia GWAS and consensus DEG genes by C3 decile. The skew of the histograms towards higher C3 deciles reflects the significant enrichment of both non-overlapping gene sets, as in Fig. 4c-d.* ***c****, Histograms of the schizophrenia GWAS and DEG genes from each separate study by C3 decile,*

596 *coloured by cortical layer where the gene was identified as a marker gene [38]. L2 genes are distinctly clustered*
597 *towards the C3+ pole, while L1 and WM genes are clustered towards C3-.* ***d****, For schizophrenia and ASD,*
598 *enrichments of the GWAS/DEG genes from each separate study for marker genes of cortical layers, showing that*
599 *no consistent significant enrichments are found across the entire gene sets for studies of either disorder.* ***e****,*
600 *Enrichments as in d, except for only genes positively weighted in C3 (corresponding to the right-hand five deciles*
601 *of each histogram in panel c). For schizophrenia, significant enrichments for L2 and L3 are observed for three of*
602 *the four DEG studies, as well as the GWAS study. No such enrichments were observed for ASD, demonstrating*
603 *that C3 reveals convergent biology across otherwise inconsistent results specifically for schizophrenia.*
604 *Significance was tested by one-sided Fisher's exact test and corrected for multiple comparisons across all tests in*
605 *each panel. *, **, *** indicate FDR-corrected one-sided p-value < 0.05, 0.01, 0.001 respectively.*

606

607 # Acknowledgements

608 The authors acknowledge and thank Sofie Valk and Varun Warrier for their helpful comments on the
609 manuscript.
610
611 R.D. was supported by the Gates Cambridge Trust. J.S. was supported by NIMH T32MH019112-29 and
612 K08MH120564. A.A. was funded by a grant from the Australian Research Council (ARC) under its
613 Linkage Project scheme (LP160101592). R.A.I.B. was supported by the Autism Research Trust. K.S.W.
614 was supported by the Wellcome Trust (215901/Z/19/Z). E.T.B. was supported by an NIHR Senior
615 Investigator award and the Wellcome Trust collaborative award for the Neuroscience in Psychiatry
616 Network (NSPN). A.R. was supported by the National Institute of Mental Health Intramural Research
617 Program (NIH Annual Report Number, 1ZIAMH002949-04). P.E.V. is a Fellow of MQ: Transforming
618 Mental Health (MQF17_24). The funders had no role in study design, data collection and analysis,
619 decision to publish or preparation of the manuscript.
620
621 Data were curated and analysed using a computational facility funded by an MRC research
622 infrastructure award (MR/M009041/1) to the School of Clinical Medicine, University of Cambridge. All
623 research at the Department of Psychiatry in the University of Cambridge is supported by the NIHR
624 Cambridge Biomedical Research Centre (BRC-1215-20014) and NIHR Applied Research Centre. The
625 views expressed are those of the authors and not necessarily those of the NIH, NHS, the NIHR or the
626 Department of Health and Social Care. For the purpose of open access, the authors have applied a
627 Creative Commons Attribution (CC BY) licence to any Author Accepted Manuscript version arising from
628 this submission.

629 # Author Contributions statement

630 P.E.V., R.D., J.S., K.W., and A.R. designed research. J.S., A.A., K.W., and R.B. contributed data. R.D. and
631 P.E.V. performed research, and E.T.B., K.A., K.W., A.R., J.S., R.M., and A.A. helped interpret results.
632 R.D., P.E.V., and E.T.B. wrote the manuscript. All authors reviewed the manuscript.

633 # Competing Interests statement

634 K.M.A. is an employee of Neumora Therapeutics. R.D.M. is an employee of Octave Biosciences. E.T.B.
635 has consulted for Boehringer Ingelheim, SR One, GlaxoSmithKline, Sosei Heptares, Monument
636 Therapeutics. All other authors have no disclosures to make.

637 # References

638 1. van den Heuvel, M. P. & Yeo, B. T. T. A spotlight on bridging microscale and macroscale human
639 brain architecture. *Neuron* **93**, 1248–1251 (2017).
640 2. Hawrylycz, M. J. *et al.* An anatomically comprehensive atlas of the adult human brain
641 transcriptome. *Nature* **489**, 391–399 (2012).
642 3. Oldham, M. C. *et al.* Functional organization of the transcriptome in human brain. *Nat.*
643 *Neurosci.* **11**, 1271–1282 (2008).
644 4. Kang, H. J. *et al.* Spatio-temporal transcriptome of the human brain. *Nature* **478**, 483–489
645 (2011).
646 5. Ayoub, A. E. *et al.* Transcriptional programs in transient embryonic zones of the cerebral
647 cortex defined by high-resolution mRNA sequencing. *Proc. Natl. Acad. Sci. U. S. A.* **108**, 14950–
648 14955 (2011).
649 6. Miller, J. A. *et al.* Transcriptional landscape of the prenatal human brain. *Nature* **508**, 199–206
650 (2014).
651 7. Bakken, T. E. *et al.* A comprehensive transcriptional map of primate brain development.
652 *Nature* **535**, 367–375 (2016).
653 8. Burt, J. B. *et al.* Hierarchy of transcriptomic specialization across human cortex captured by
654 structural neuroimaging topography. *Nat. Neurosci.* **21**, 1251–1259 (2018).
655 9. Fulcher, B. D., Murray, J. D., Zerbi, V. & Wang, X.-J. Multimodal gradients across mouse cortex.
656 *Proc. Natl. Acad. Sci. U. S. A.* **116**, 4689–4695 (2019).
657 10.Sydnor, V. J. *et al.* Neurodevelopment of the association cortices: Patterns, mechanisms, and
658 implications for psychopathology. *Neuron* **109**, 2820–2846 (2021).
659 11.Rayon, T., Maizels, R. J., Barrington, C. & Briscoe, J. Single-cell transcriptome profiling of the
660 human developing spinal cord reveals a conserved genetic programme with human-specific
661 features. *Development* **148**, (2021).
662 12.Kudo, L. C., Karsten, S. L., Chen, J., Levitt, P. & Geschwind, D. H. Genetic analysis of anterior

663 posterior expression gradients in the developing mammalian forebrain. *Cereb. Cortex* **17**, 2108–
664 2122 (2007).
665 13.Polleux, F., Ince-Dunn, G. & Ghosh, A. Transcriptional regulation of vertebrate axon guidance
666 and synapse formation. *Nat. Rev. Neurosci.* **8**, 331–340 (2007).
667 14.Krienen, F. M. *et al.* Innovations present in the primate interneuron repertoire. *Nature* **586**,
668 262–269 (2020).
669 15.Goyal, M. S., Hawrylycz, M., Miller, J. A., Snyder, A. Z. & Raichle, M. E. Aerobic glycolysis in the
670 human brain is associated with development and neotenous gene expression. *Cell Metab.* **19**, 49–
671 57 (2014).
672 16.Huntenburg, J. M., Bazin, P.-L. & Margulies, D. S. Large-scale gradients in human cortical
673 organization. *Trends Cogn. Sci.* **22**, 21–31 (2018).
674 17.Margulies, D. S. *et al.* Situating the default-mode network along a principal gradient of
675 macroscale cortical organization. *Proc. Natl. Acad. Sci. U. S. A.* **113**, 12574–12579 (2016).
676 18.Hill, J. *et al.* Similar patterns of cortical expansion during human development and evolution.
677 *Proc. Natl. Acad. Sci. U. S. A.* **107**, 13135–13140 (2010).
678 19.Goulas, A., Margulies, D. S., Bezgin, G. & Hilgetag, C. C. The architecture of mammalian cortical
679 connectomes in light of the theory of the dual origin of the cerebral cortex. *Cortex* **118**, 244–261
680 (2019).
681 20.Morgan, S. E. *et al.* Cortical patterning of abnormal morphometric similarity in psychosis is
682 associated with brain expression of schizophrenia-related genes. *Proc. Natl. Acad. Sci. U. S. A.*
683 **116**, 9604–9609 (2019).
684 21.Romero-Garcia, R., Warrier, V., Bullmore, E. T., Baron-Cohen, S. & Bethlehem, R. A. I. Synaptic
685 and transcriptionally downregulated genes are associated with cortical thickness differences in
686 autism. *Mol. Psychiatry* **24**, 1053–1064 (2019).
687 22.Seidlitz, J. *et al.* Transcriptomic and cellular decoding of regional brain vulnerability to
688 neurogenetic disorders. *Nat. Commun.* **11**, 3358 (2020).

689 23.Romero-Garcia, R. *et al.* Schizotypy-related magnetization of cortex in healthy adolescence Is
690 colocated with expression of schizophrenia-related genes. *Biol. Psychiatry* **88**, 248–259 (2020).
691 24.Anderson, K. M. *et al.* Transcriptional and imaging-genetic association of cortical interneurons,
692 brain function, and schizophrenia risk. *Nat. Commun.* **11**, 2889 (2020).
693 25.Anderson, K. M. *et al.* Convergent molecular, cellular, and cortical neuroimaging signatures of
694 major depressive disorder. *Proc. Natl. Acad. Sci. U. S. A.* **117**, 25138–25149 (2020).
695 26.Fornito, A., Arnatkevičiūtė, A. & Fulcher, B. D. Bridging the gap between connectome and
696 transcriptome. *Trends Cogn. Sci.* **23**, 34–50 (2019).
697 27.Arnatkeviciute, A., Fulcher, B., Bellgrove, M. & Fornito, A. Imaging transcriptomics of brain
698 disorders. *PsyArXiv* (2021) doi:10.31234/osf.io/4exug.
699 28.Martins, D. *et al.* Imaging transcriptomics: Convergent cellular, transcriptomic, and molecular
700 neuroimaging signatures in the healthy adult human brain. *Cell Rep.* **37**, 110173 (2021).
701 29.Voineskos, A. N. *et al.* Effects of antipsychotic medication on brain structure in patients with
702 major depressive disorder and psychotic features: neuroimaging findings in the context of a
703 randomized placebo-controlled clinical trial. *JAMA Psychiatry* **77**, 674–683 (2020).
704 30.Perzel Mandell, K. A. *et al.* Molecular phenotypes associated with antipsychotic drugs in the
705 human caudate nucleus. *Mol. Psychiatry* **27**, 2061–2067 (2022).
706 31.Schulmann, A. *et al.* Antipsychotic drug use complicates assessment of gene expression
707 changes associated with schizophrenia. *Transl. Psychiatry* **13**, 93 (2023).
708 32.Glasser, M. F. *et al.* A multi-modal parcellation of human cerebral cortex. *Nature* **536**, 171–178
709 (2016).
710 33.Arnatkevičiūtė, A., Fulcher, B. D. & Fornito, A. A practical guide to linking brain-wide gene
711 expression and neuroimaging data. *Neuroimage* **189**, 353–367 (2019).
712 34.Markello, R. D. *et al.* Standardizing workflows in imaging transcriptomics with the abagen
713 toolbox. *bioRxiv* 2021.07.08.451635 (2021) doi:10.1101/2021.07.08.451635.
714 35.Hawrylycz, M. *et al.* Canonical genetic signatures of the adult human brain. *Nat. Neurosci.* **18**,

715 1832–1844 (2015).
716 36.Gandal, M. J. *et al.* Broad transcriptomic dysregulation occurs across the cerebral cortex in
717 ASD. *Nature* **611**, 532–539 (2022).
718 37.Moran, P. A. P. Notes on continuous stochastic phenomena. *Biometrika* **37**, 17–23 (1950).
719 38.Maynard, K. R. *et al.* Transcriptome-scale spatial gene expression in the human dorsolateral
720 prefrontal cortex. *Nat. Neurosci.* **24**, 425–436 (2021).
721 39.Lee, J. J. *et al.* Gene discovery and polygenic prediction from a genome-wide association study
722 of educational attainment in 1.1 million individuals. *Nat. Genet.* **50**, 1112–1121 (2018).
723 40.Davies, G. *et al.* Study of 300,486 individuals identifies 148 independent genetic loci
724 influencing general cognitive function. *Nat. Commun.* **9**, 2098 (2018).
725 41.Hill, W. D. *et al.* A combined analysis of genetically correlated traits identifies 187 loci and a
726 role for neurogenesis and myelination in intelligence. *Mol. Psychiatry* **24**, 169–181 (2019).
727 42.Savage, J. E. *et al.* Genome-wide association meta-analysis in 269,867 individuals identifies
728 new genetic and functional links to intelligence. *Nat. Genet.* **50**, 912–919 (2018).
729 43.Hatoum, A. S. *et al.* Genome-wide association study shows that executive functioning is
730 influenced by GABAergic processes and is a neurocognitive genetic correlate of psychiatric
731 disorders. *Biol. Psychiatry* **93**, 59–70 (2023).
732 44.Lake, B. B. *et al.* Integrative single-cell analysis of transcriptional and epigenetic states in the
733 human adult brain. *Nat. Biotechnol.* **36**, 70–80 (2018).
734 45.Glasser, M. F. & Van Essen, D. C. Mapping human cortical areas in vivo based on myelin
735 content as revealed by T1- and T2-weighted MRI. *J. Neurosci.* **31**, 11597–11616 (2011).
736 46.Van Essen, D. C. *et al.* The WU-Minn Human Connectome Project: an overview. *Neuroimage*
737 **80**, 62–79 (2013).
738 47.Vaishnavi, S. N. *et al.* Regional aerobic glycolysis in the human brain. *Proc. Natl. Acad. Sci. U. S.*
739 *A.* **107**, 17757–17762 (2010).
740 48.Satterthwaite, T. D. *et al.* Impact of puberty on the evolution of cerebral perfusion during

741 adolescence. *Proc. Natl. Acad. Sci. U. S. A.* **111**, 8643–8648 (2014).

742 49. Reardon, P. K. *et al.* Normative brain size variation and brain shape diversity in humans.
743 *Science* **360**, 1222–1227 (2018).

744 50. Paquola, C. *et al.* A multi-scale cortical wiring space links cellular architecture and functional
745 dynamics in the human brain. *PLoS Biol.* **18**, e3000979 (2020).

746 51. Yarkoni, T., Poldrack, R. A., Nichols, T. E., Van Essen, D. C. & Wager, T. D. Large-scale
747 automated synthesis of human functional neuroimaging data. *Nat. Methods* **8**, 665–670 (2011).

748 52. Mesulam, M.-M. *Principles of behavioral neurology*. (Oxford University Press, USA, 1985).

749 53. Glasser, M. F. *et al.* The Human Connectome Project's neuroimaging approach. *Nat. Neurosci.*
750 **19**, 1175–1187 (2016).

751 54. Paquola, C. *et al.* Shifts in myeloarchitecture characterise adolescent development of cortical
752 gradients. *Elife* **8**, (2019).

753 55. Larson-Prior, L. J. *et al.* Adding dynamics to the Human Connectome Project with MEG.
754 *Neuroimage* **80**, 190–201 (2013).

755 56. Whitaker, K. J. *, Vértes, P. E. *. *et al.* Adolescence is associated with genomically patterned
756 consolidation of the hubs of the human brain connectome. *Proc. Natl. Acad. Sci. U. S. A.* **113**,
757 9105–9110 (2016).

758 57. Váša, F. *et al.* Conservative and disruptive modes of adolescent change in human brain
759 functional connectivity. *Proc. Natl. Acad. Sci. U. S. A.* **117**, 3248–3253 (2020).

760 58. Hodge, R. D. *et al.* Conserved cell types with divergent features in human versus mouse
761 cortex. *Nature* **573**, 61–68 (2019).

762 59. Bethlehem, R. A. I. *et al.* Brain charts for the human lifespan. *Nature* **604**, 525–533 (2022).

763 60. Matoba, N. *et al.* Common genetic risk variants identified in the SPARK cohort support DDHD2
764 as a candidate risk gene for autism. *Transl. Psychiatry* **10**, 265 (2020).

765 61. Howard, D. M. *et al.* Genome-wide meta-analysis of depression identifies 102 independent
766 variants and highlights the importance of the prefrontal brain regions. *Nat. Neurosci.* **22**, 343–352

767 (2019).
768 62.Trubetskoy, V. *et al.* Mapping genomic loci implicates genes and synaptic biology in
769 schizophrenia. *Nature* **604**, 502–508 (2022).
770 63.Wagstyl, K. *et al.* Multiple markers of cortical morphology reveal evidence of supragranular
771 thinning in schizophrenia. *Transl. Psychiatry* **6**, e780 (2016).
772 64.Parikshak, N. N. *et al.* Genome-wide changes in lncRNA, splicing, and regional gene expression
773 patterns in autism. *Nature* **540**, 423–427 (2016).
774 65.Gandal, M. J. *et al.* Transcriptome-wide isoform-level dysregulation in ASD, schizophrenia, and
775 bipolar disorder. *Science* **362**, (2018).
776 66.Jaffe, A. E. *et al.* Decoding shared versus divergent transcriptomic signatures across cortico-
777 amygdala circuitry in PTSD and depressive disorders. *Am. J. Psychiatry* **179**, 673–686 (2022).
778 67.Fromer, M. *et al.* Gene expression elucidates functional impact of polygenic risk for
779 schizophrenia. *Nat. Neurosci.* **19**, 1442–1453 (2016).
780 68.Birnbaum, R. *et al.* Investigating the neuroimmunogenic architecture of schizophrenia. *Mol.*
781 *Psychiatry* **23**, 1251–1260 (2018).
782 69.Collado-Torres, L. *et al.* Regional heterogeneity in gene expression, regulation, and coherence
783 in the frontal cortex and hippocampus across development and schizophrenia. *Neuron* **103**, 203–
784 216.e8 (2019).
785 70.Jaffe, A. E. *et al.* Developmental and genetic regulation of the human cortex transcriptome
786 illuminate schizophrenia pathogenesis. *Nat. Neurosci.* **21**, 1117–1125 (2018).
787 71.de Leeuw, C. A., Mooij, J. M., Heskes, T. & Posthuma, D. MAGMA: generalized gene-set
788 analysis of GWAS data. *PLoS Comput. Biol.* **11**, e1004219 (2015).
789 72.Sey, N. Y. A. *et al.* A computational tool (H-MAGMA) for improved prediction of brain-disorder
790 risk genes by incorporating brain chromatin interaction profiles. *Nat. Neurosci.* **23**, 583–593
791 (2020).
792 73.Merikangas, A. K. *et al.* What genes are differentially expressed in individuals with

793 schizophrenia? A systematic review. *Mol. Psychiatry* **27**, 1373–1383 (2022).
794 74.Hilgetag, C. C., Goulas, A. & Changeux, J.-P. A natural cortical axis connecting the outside and
795 inside of the human brain. *Netw Neurosci* **6**, 950–959 (2022).
796 75.Senoussi, M. *et al.* Theta oscillations shift towards optimal frequency for cognitive control. *Nat*
797 *Hum Behav* **6**, 1000–1013 (2022).
798 76.Pizzagalli, D. A., Oakes, T. R. & Davidson, R. J. Coupling of theta activity and glucose
799 metabolism in the human rostral anterior cingulate cortex: an EEG/PET study of normal and
800 depressed subjects. *Psychophysiology* **40**, 939–949 (2003).
801 77.Choudhury, S., Charman, T. & Blakemore, S.-J. Development of the teenage brain. *Mind Brain*
802 *Educ.* **2**, 142–147 (2008).
803 78.Brenhouse, H. C. & Schwarz, J. M. Immunoadolescence: Neuroimmune development and
804 adolescent behavior. *Neurosci. Biobehav. Rev.* **70**, 288–299 (2016).
805 79.Bellenguez, C. *et al.* New insights into the genetic etiology of Alzheimer's disease and related
806 dementias. *Nat. Genet.* **54**, 412–436 (2022).
807 80.Faust, T. E., Gunner, G. & Schafer, D. P. Mechanisms governing activity-dependent synaptic
808 pruning in the developing mammalian CNS. *Nat. Rev. Neurosci.* **22**, 657–673 (2021).
809 81.Kalish, B. T. *et al.* Single-cell transcriptomics of the developing lateral geniculate nucleus
810 reveals insights into circuit assembly and refinement. *Proc. Natl. Acad. Sci. U. S. A.* **115**, E1051–
811 E1060 (2018).
812 82.Feinberg, I. Schizophrenia: caused by a fault in programmed synaptic elimination during
813 adolescence? *J. Psychiatr. Res.* **17**, 319–334 (1982).
814 83.Johnson, M. B. & Hyman, S. E. A critical perspective on the synaptic pruning hypothesis of
815 schizophrenia pathogenesis. *Biol. Psychiatry* **92**, 440–442 (2022).
816 84.Howes, O. D. & Onwordi, E. C. The synaptic hypothesis of schizophrenia version III: a master
817 mechanism. *Mol. Psychiatry* (2023) doi:10.1038/s41380-023-02043-w.
818 85.Harrison, P. J. & Weinberger, D. R. Schizophrenia genes, gene expression, and neuropathology:

819 on the matter of their convergence. *Mol. Psychiatry* **10**, 40–68; image 5 (2005).

820 86.Kleinman, J. E. *et al.* Genetic neuropathology of schizophrenia: new approaches to an old
821 question and new uses for postmortem human brains. *Biol. Psychiatry* **69**, 140–145 (2011).

822 87.Semendeferi, K., Armstrong, E., Schleicher, A., Zilles, K. & Van Hoesen, G. W. Prefrontal cortex
823 in humans and apes: a comparative study of area 10. *Am. J. Phys. Anthropol.* **114**, 224–241
824 (2001).

825 88.Hutsler, J. J., Lee, D.-G. & Porter, K. K. Comparative analysis of cortical layering and
826 supragranular layer enlargement in rodent carnivore and primate species. *Brain Res.* **1052**, 71–81
827 (2005).

828 89.Galakhova, A. A. *et al.* Evolution of cortical neurons supporting human cognition. *Trends Cogn.*
829 *Sci.* **26**, 909–922 (2022).

830 90.Petanjek, Z. *et al.* Extraordinary neoteny of synaptic spines in the human prefrontal cortex.
831 *Proc. Natl. Acad. Sci. U. S. A.* **108**, 13281–13286 (2011).

832 91.Heyer, D. B. *et al.* Verbal and general IQ associate with supragranular layer thickness and cell
833 properties of the left temporal cortex. *Cereb. Cortex* **32**, 2343–2357 (2022).

834 92.Chance, S. A., Walker, M. & Crow, T. J. Reduced density of calbindin-immunoreactive
835 interneurons in the planum temporale in schizophrenia. *Brain Res.* **1046**, 32–37 (2005).

836 93.Cullen, T. J. *et al.* Anomalies of asymmetry of pyramidal cell density and structure in
837 dorsolateral prefrontal cortex in schizophrenia. *Br. J. Psychiatry* **188**, 26–31 (2006).

838 94.Batiuk, M. Y. *et al.* Upper cortical layer-driven network impairment in schizophrenia. *Sci Adv* **8**,
839 eabn8367 (2022).

840 95.Viñuela, A. *et al.* Age-dependent changes in mean and variance of gene expression across
841 tissues in a twin cohort. *Hum. Mol. Genet.* **27**, 732–741 (2018).

Methods

AHBA data and donor-level parcellation images

Probe-level gene expression data with associated spatial coordinates were obtained from the Allen Institute website (https://human.brain-map.org), which collected the data after obtaining informed consent from the deceased's next-of-kin. HCP-MMP1.0 parcellation images matched to the individual native MRI space of each donor brain (N=6) were obtained from Arnatkevičiūtė *et al.* (https://figshare.com/articles/dataset/AHBAdata/6852911) [33]. The use of native donor parcellation images (rather than a standard parcellation image with sample coordinates mapped to MNI space) was chosen as it optimised the triplet generalisability metric (see following).

AHBA processing parameters

To correctly match AHBA samples to regions in native donor space parcellation images using published processing pipelines, we recommend the use of either (i) *abagen* version 0.1.3 or greater (for Python) [34], or (ii) the version of the *AHBAprocessing* pipeline updated in June 2021 or later (for Matlab) [33].

Here we processed the AHBA with the *abagen* package, with one modification: we filtered the AHBA samples for only those annotated as cortical samples prior to subsequent processing steps. This was done such that subcortical and brainstem samples did not influence the intensity filter and probe aggregation steps. This modification was chosen as it optimised the triplet generalisability metric (see following). The code used to apply the modification is available in the *code/processing_helpers.py* file at https://github.com/richardajdear/AHBA_gradients.

Other than this modification, *abagen* was run using the following parameters, which follow published recommendations [33] unless otherwise specified:

- *Hemisphere*: The right hemisphere samples that are present for two of the six donors were reflected along the midline and processed together with the left hemisphere samples of those donor datasets to increase sample coverage.
- *Intensity-based filter*: Probes were filtered to retain only those exceeding background noise (as defined by the binary flag provided with the data by the Allen Institute) in at least 50% of the samples [33].
- *Probe aggregation*: Probes were aggregated to genes by differential stability, meaning that for each gene, the probe with the highest mean correlation across donor pairs was used.

873 - *Distance threshold*: Samples were matched to regions with a tolerance threshold of 2mm,
874 using the voxel-mass algorithm in the *abagen* package.
875 - *Sample normalisation*: Prior to aggregating over donors, samples were normalised across all
876 genes, using the scaled robust sigmoid method (a sigmoid transformation that is robust to
877 outliers [33]).
878 - *Gene normalisation*: Prior to aggregating over donors, genes were normalised across all
879 samples, again using the scaled robust sigmoid.
880

881 To ensure robustness, the primary analysis of computing components of the AHBA was repeated in a
882 series of sensitivity analyses varying all of the processing parameters above, e.g. not mirroring right
883 hemisphere samples to the left hemisphere, different or no intensity filter for genes, different
884 methods for aggregating and normalising probes. Sensitivity analyses also included running the
885 pipeline with alternative parcellation templates: HCP-MMP1.0 [32], Schaefer-400 [96], Desterieux [97], and
886 Desikan-Killiany [98]. (**Extended Data Fig. 2**).

887 Gene filtering by differential stability

888 Genes were filtered for those that showed more similar spatial patterns of expression across the six
889 donors using the metric of differential stability (DS) as previously described by Hawrylycz *et al.* [35]. For
890 each gene, DS was calculated as the average correlation of that gene's regional expression vector
891 between each donor pair (15 pairs with all six brains, or 3 pairs in the triplets analysis, see below).
892 Genes were ranked by DS and then only the top 50% percent of genes were retained. The 50%
893 threshold was chosen on the basis of a grid-search (in combination with the region filter to optimise
894 for generalisability) where the threshold for DS was varied between 10% and 100% (**Extended Data**
895 **Fig. 1**).

896 Filtering regions by donors represented

897 Regions were filtered for those that included samples from at least three of the six AHBA donor brains,
898 which in the HCP-MMP1.0 parcellation retained 137/180 regions. Note that in the triplets analysis (see
899 below), this means only brain regions with samples from all three donors in the triplet were retained.
900 The choice to filter for representation of three of the six donors was chosen on the basis of a grid-
901 search in combination with the differential stability gene filter to optimise for generalisability
902 (**Extended Data Fig. 1**).

903 ## Triplets analysis: disjoint triplet correlation as a proxy for generalisability

904 To test for generalizability we separated the six AHBA brains into pairs of disjoint triplets (for example
905 donor brains 1,2,3 in one triplet and 4,5,6 in another). We applied our full analysis pipeline (including
906 all processing steps e.g. probe aggregation, normalisation, and filters) independently to each of the
907 twenty possible combinations of triplets, and correlated the regional scores for each DME or PCA
908 component between each of the ten disjoint pairs (Pearson's *r*). When filtering for consistently-
909 sampled regions, the retained regions were different for each triplet of donor brains, so correlations
910 were performed on only the intersection of regions retained in both triplets of each pair.
911
912 As the order of principal components can vary across different triplets, we employed a matching
913 algorithm in which the full correlation matrix was computed between the top 5 principal components
914 of both triplets (e.g. C1 from triplet A was correlated with each of C1-C5 of triplet B). The highest
915 absolute correlation value in the matrix was then identified as representing two matched components
916 and removed from the matrix, with the process repeated until all components were matched. The
917 components were then ranked by the mean variance explained in each matched pair.
918
919 The median absolute correlation across all ten disjoint triplet pairs represented the generalisability, *g*,
920 of the AHBA components processed using the given set of parameters. Processing parameters, in
921 particular the filters for regions and donors, were optimised so as to maximise *g* while retaining as
922 many genes and regions as possible; see **Extended Data Fig. 1**.

923 ## Dimension reduction methods

924 Dimension reduction was performed using both principal component analysis (PCA) and diffusion map
925 embedding (DME), the latter having been described for use in spatial gradient analysis of brain
926 imaging data by Margulies *et al.* [17]. For DME, the normalised cosine function was used as the kernel
927 for the affinity matrix. No sparsity was added, and the alpha parameter was set at 1. These
928 parameters were chosen as they optimised the inter-triplet correlation metric for generalisability.
929 Both PCA and DME methods were implemented using the BrainSpace package [99]. See Supplementary
930 Methods for further explanation on DME and its benefits over PCA and other alternatives (e.g. ICA).
931

932 ## Component gene weights

933 For each component, gene weights were computed as the Pearson correlation of each gene's
934 individual spatial expression vector with the regional scores of the component. For PCA these

935 correlations are equivalent to the PCA loadings (eigenvectors) multiplied by the square root of the
936 variance explained by the component (eigenvalues).

937 Variance explained

938 For PCA, variance explained is given directly by the squared eigenvalues of the singular value
939 decomposition. For DME, eigenvalues do not represent variance explained as the gene expression
940 matrix is first converted to an affinity matrix using a kernel (here the normalized cosine). Therefore,
941 variance explained was calculated as the difference in the total variance of the region-by-gene
942 expression matrix before and after regressing the matrix on each component's region scores.
943
944 That is, defining the residual regional expression vector of gene *g* after regressing out *i* components as
945 $e_{g,i}$, the total variance V_i of the residualised region-by-gene expression matrix is

$$V_i = \sum_g \quad Var(e_{g,i})$$

946 and for each component C_i, variance explained VE_i is given by

947 $$VE_i = V_{i-1} - V_i \ .$$

948 Gene Ontology enrichment analysis for biological processes

949 Biological process enrichments of the gene weights for each component were computed using the
950 'proteins with values/ranks' function of online software *STRING* [103], which tests whether the mean
951 weight of each annotated gene list is significantly higher or lower than random permutations of the
952 same gene weights (the "aggregate fold change" method [103,104]), and includes a Benjamini-Hochberg
953 adjustment of the False Discovery Rate (FDR).
954
955 The aggregate fold change method was chosen as it does not require thresholding the gene weights of
956 the components to define 'target' vs 'background' gene lists (as in e.g. Fisher's exact test). That is,
957 rather than setting a threshold for which genes are 'in' or 'out' of each component, we took the
958 weighted gene list where all genes can have some contribution to each component, and for each
959 component tested whether each Gene Ontology gene list was in aggregate more positively- or
960 negatively-weighted than chance.
961

Layer and cell-type enrichment analyses

The gene lists for cortical layer marker genes were obtained from published analyses of laminar enrichment in spatial transcriptomic data from human postmortem tissue in the dorsolateral prefrontal cortex [38] (columns Q-W of Table S4B in Maynard *et al.* [38]).

Cell-type gene lists were obtained from Seidlitz *et al.* [22], who compiled lists of significantly differentially expressed genes from five independent single-cell RNA-seq studies [44,105–108]. The gene list for synaptic marker genes was the unfiltered gene list from SynaptomeDB [109].

All enrichments for layers and cell-types were computed by the same aggregate fold change method [104] as in the *STRING* software [103], whereby the mean gene weight of each gene list was computed for both the true set of gene weights of each component, and for 5,000 random permutations of the weights. The *Z*-scores and permutation test *P*-values for significance testing of enrichment were corrected for multiple comparisons with the Benjamini-Hochberg FDR.

GWAS enrichment analyses for educational attainment and intelligence

Genes associated with cognitive capacity by GWAS were obtained from:

- Lee *et al.* 2018, Supplementary Table 7 [39] (educational attainment).
- Davies *et al.* 2018, Supplementary Table 6 [40]
- Savage *et al.* 2018, Supplementary Table 15 [42]
- Hill *et al.* 2019, Supplementary Table 5 [41]
- Hatoum *et al.* 2023, Supplementary Table 16 [43]

Enrichment tests were performed by the aggregate fold change method [104], as above.

Neuroimaging and other macro-scale brain maps (Fig. 2)

Neuroimaging and other macro-scale maps were obtained as follows:

- The 9 neuroimaging and macro-scale maps in the clustering analysis (**Fig. 2a**) were obtained from the *Neuromaps* package [110], and are also available in Sydnor *et al.* [10].
- The regions of cytoarchitectural differentiation (**Fig. 2b**) were obtained from Paquola *et al.* 2019 [111] and averaged into the HCP-MMP parcellation using the *Neuromaps* package [110].
- The map of fMRI degree (**Fig. 2c**) was obtained from Paquola *et al.* 2020 [50], and was originally computed from the HCP S900 release [112].

993 - The maps of MEG power bands (**Fig. 2d, Extended Data Fig. 5**) were obtained from the
994 *Neuromaps* package [110].
995 - The map of adolescent change in cortical myelination was obtained from Váša *et al.* 2020 [57].
996
997 All maps were aggregated into HCP-MMP parcellation, and are provided in **Supplementary Table 3**.
998
999 Spatial associations between maps and the transcriptional components were computed by Pearson
1000 correlations and tested for significance using spin permutation tests (5,000 spins) by the Cornblath
1001 method [113], leveraging tools from *Neuromaps* [110], and tested for significance with FDR correction for
1002 multiple testing.
1003
1004 For the regions of cytoarchitectural differentiation, the mean component scores in each architectonic
1005 class were tested for differences between class mean scores using analysis of variance (ANOVA)
1006 against spin-permuted null models, followed by correction for FDR. The associations between
1007 individual cytoarchitectural regions and each component were computed by the Z-score of the mean
1008 component score in each region normalised by a spin permutation distribution of the regional mean
1009 component score with significance testing corrected for FDR.

1010 Single-cell co-variation analysis (Fig. 3a)

1011 Single-cell RNA-seq data were obtained from the Allen Cell Types Database (https://portal.brain-
1012 map.org/atlases-and-data/rnaseq) [58].
1013
1014 Single-cell gene expression was filtered for the 7,873 genes in the optimally filtered AHBA dataset. To
1015 perform the analysis in **Fig. 3a**, the positive and negative gene weights were separated for each of C1-
1016 C3, and the dot product taken with the gene expression matrix of single-cell samples. This produced a
1017 vector of six numbers, representing the weighted total expression of C1+, C1-, C2+, C2-, C3+, C3- genes
1018 respectively, for each of the 50,000 single-cell samples.
1019
1020 That is, given the gene expression vector s_j of each single-cell sample *j*, we computed the total
1021 weighted positive and negative expression $s^+{}_{j,Ci}$ and $s^-{}_{j,Ci}$ from the C1-C3 gene weights as:

1022 $$s^+{}_{j,Ci} = s_j \cdot u^+{}_{Ci} \quad \text{and} \quad s^-{}_{j,Ci} = s_j \cdot u^-{}_{Ci}$$

1023 where $u^+{}_{Ci} = max\{u_{Ci}, 0\}$ and $u^-{}_{Ci} = min\{u_{Ci}, 0\}$.

BrainSpan developmental gene expression processing (Fig. 3b-d)

BrainSpan data were obtained directly from the Allen Institute website [6] (http://brainspan.org) and processed as follows:

1. The 11 cortical regions in the BrainSpan data were manually matched to the HCP-MMP1.0 parcellation regions according to the descriptions in the BrainSpan documentation. This mapping is provided online at https://github.com/richardajdear/AHBA_gradients.
2. Exon-level expression data were filtered for only the matched BrainSpan regions.
3. Donor brains from which fewer than 4 regions were sampled were dropped.
4. Within each donor, expression of each gene was Z-normalised over regions.
5. Donors were aggregated into three age ranges (pre-birth, birth-13 years, and 18-40 years) and expression was averaged for each gene.

AHBA-BrainSpan developmental consistency analysis (Fig. 3b-d)

Consistency between the AHBA components and BrainSpan was evaluated as follows:

1. Processed BrainSpan data were filtered for only the 7,973 genes retained in the filtered AHBA dataset (top 50% by differential stability; see above).
2. The dot product of the gene weights for C1-C3 were taken against the BrainSpan data, resulting in 'BrainSpan scores' for each of C1-C3, for each of the 11 BrainSpan regions, at each age range (pre-birth, birth-13 years, and 18-40 years).
3. In each of the 11 BrainSpan regions, 'AHBA scores' were computed as the mean of the matching HCP-MMP region scores from the original C1-C3 maps derived from the AHBA.
4. The 'BrainSpan scores' and 'AHBA scores' were correlated over the 11 BrainSpan regions (Pearson's *r*), for each of C1-C3 and for each age bucket of the BrainSpan data.

As further clarification: given gene weights u_i for AHBA component C_i and the vector of expression over genes b_j for each BrainSpan sample *j* (with a given age and region), the 'BrainSpan score' is

$$y_{j,i} = b_j \cdot u_i$$

and the consistency was tested as the correlation across the matched regions of the AHBA scores *x* and the mean of the BrainSpan scores $\underline{y}$ of BrainSpan donors in each age range.

BrainSpan developmental trajectory modelling (Fig. 3e)

The developmental trajectories of each decile of C1-C3 were computed as follows:

1. The ages in the BrainSpan data were converted to post-conception days on a log10 scale.

1055 2. For each gene, a Generalised Additive Model was fitted using the *GLMGam* function in the
1056 *statsmodels* python package with alpha=1, and 12 3rd-degree basis splines as a smoothing
1057 function (df=12, degree=3 in the *BSplines* function). Sex and brain region were included as
1058 covariates.
1059 3. Developmental curves were plotted from the fitted models for each gene, sex, and region,
1060 then averaged by decile of gene weight for each of C1-C3.

1061 Disorder spatial associations (Fig. 4a-b)

1062 Maps of the regional centile score differences in cortical volume for ASD, MDD, and schizophrenia
1063 were obtained from the BrainCharts project by Bethlehem, Seidlitz, White *et al.* [59], in which normative
1064 models were computed for multiple brain phenotypes across the human lifespan from a harmonised
1065 dataset of >125,000 total MRI scans ($N_{controls}$ = 38,839, N_{ASD} = 381, N_{MDD} = 3,861, N_{SCZ} = 315). As these
1066 data were in the Desikan-Killiany parcellation, the AHBA components in the HCP-MMP parcellation
1067 were mapped to a vertex-level surface map (FreeSurfer's 41k fsaverage atlas) then re-averaged into
1068 the Desikan-Killiany parcellation. Pearson correlations with cortical maps of C1-C3 scores were
1069 computed, significance was assessed by spin permutation tests, and corrected for FDR across all nine
1070 tests (three disorders by three components).
1071
1072 These disorder maps are provided in **Supplementary Table 4**.

1073 Disorder DEG associations (Fig. 4c)

1074 Differentially expressed genes (DEGs; FDR < 5%) from RNA-seq of postmortem brain tissue were
1075 obtained from the following case-control studies for each of ASD, MDD, and schizophrenia:
1076 - ASD:
1077 - Gandal *et al.* 2022, Supplementary Table S3 [36], WholeCortex_ASD_FDR < 0.05
1078 - Gandal *et al.* 2018, Supplementary Table S1 [65], ASD.fdr < 0.05
1079 - Parikshak *et al.* 2016, Supplementary Table S2 [64], FDR-adjusted P value, ASD vs CTL <
1080 0.05
1081 - MDD
1082 - Jaffe *et al.* 2022, Supplementary Table S2 [66], Cortex_adjPVal_MDD < 0.05
1083 - Schizophrenia
1084 - Fromer *et al.* 2016, Supplementary Table S16 [67], FDR estimate < 0.05
1085 - Gandal *et al.* 2018, Supplementary Table S1 [65], SCZ.fdr < 0.05
1086 - Jaffe *et al.* 2018, Supplementary Table S9 [70], fdr_qsva < 0.05

1087 - Collado-Torres *et al.* 2019, Supplementary Table S11 [69], adj.P.Val < 0.05 & region ==
1088 'DLPFC'
1089
1090 A consensus list of DEGs was compiled for each disorder (except MDD where only one study was
1091 included) by including only those genes identified in at least 2 studies.
1092
1093 Enrichments for these gene sets in each disorder were computed by the aggregate fold change
1094 method [104], i.e. computing the percentile of the mean weight of the DEGs in C1-C3 relative to the
1095 5,000 random permutations of the gene labels.

1096 Disorder-associated genes from GWAS (Fig. 4d)

1097 Genes significantly associated with ASD, MDD, and schizophrenia by GWAS were obtained from:
1098 - ASD: Matoba *et al.* 2020, Supplementary Table S7 [60]
1099 - MDD: Howard *et al.* 2019, Supplementary Table S9 [61]
1100 - Schizophrenia: Trubetskoy *et al.* 2022, Extended GWAS [62]:
1101 https://figshare.com/articles/dataset/scz2022/19426775?file=35775617
1102
1103 Associations with GWAS were calculated using three methods (**Supplementary Figure S6**):
1104 - Enrichment of the prioritised genes identified in each of the specific studies, using the
1105 aggregate fold change method [104] as described above.
1106 - MAGMA [71], a regression technique which tests for association between each of the
1107 components C1-C3 and the *P*-values for each gene's association with ASD, MDD or SCZ (from
1108 corresponding primary GWAS studies) without requiring a threshold to be applied to the
1109 GWAS-derived *P*-values to define a prioritised subset of genes for enrichment analysis.
1110 MAGMA additionally accounts for gene length and gene-gene correlations. The COVAR
1111 function of MAGMA was used to test for association of the GWAS *P*-values with the C1-C3
1112 gene weights as a continuous variable. For standard MAGMA, a SNP-to-gene mapping window
1113 of +35kb/-10kb was used.
1114 - H-MAGMA [72], an extension of MAGMA where SNP-to-gene mapping is performed using Hi-C
1115 chromatin measurements from postmortem brain tissue so as to capture trans-regulatory
1116 effects. We used the Hi-C mapping from adult brain DLPFC available online from the original
1117 H-MAGMA authors.

1118 ### Laminar enrichments shared across DEG and GWAS gene sets (Fig. 4f)

1119 Enrichments for the marker genes of each cortical layer [38] were computed for the disorder-associated
1120 gene lists from DEGs and GWAS using Fisher's exact test. These enrichments were computed both
1121 with and without filtering for only genes with positive C3 weights.

1122 ### Schizophrenia supragranular-specific cortical thinning (Fig. 4g)

1123 The MRI-derived map of supragranular cortical thinning in schizophrenia was obtained from Wagstyl
1124 *et al.* [63] (N=90 subjects, 46 cases), and parcellated using the HCP-MMP1.0 parcellation. Pearson's
1125 correlations were computed with C1-C3 and significance assessed by spin permutation tests, corrected
1126 for FDR.
1127
1128

1129 ## Data availability

1130 Regional scores and gene weights for the transcriptional components C1-C3 are provided in
1131 **Supplementary Table 1**.
1132
1133 Gene expression datasets used are all publicly available:
1134 - The Allen Human Brain Atlas is available at http://human.brain-map.org, and individual donor
1135 HCP-MMP parcellation images at https://figshare.com/articles/dataset/AHBAdata/6852911.
1136 - The BrainSpan Atlas is available at https://www.brainspan.org/.
1137 - The Allen Human Cell Atlas is available at https://portal.brain-map.org/atlases-and-
1138 data/rnaseq.
1139 - The PsychENCODE dataset is available at https://github.com/dhglab/Broad-transcriptomic-
1140 dysregulation-across-the-cerebral-cortex-in-ASD.
1141
1142 Neuroimaging maps of healthy brain features are available in the neuromaps package
1143 (https://github.com/netneurolab/neuromaps). For convenience all brain maps used are provided in
1144 **Supplementary Table 3-4**. Gene lists used for enrichment analyses were all obtained from prior
1145 publications as detailed in **Methods**.
1146

1147 # Code availability

1148 Analyses were performed with Python v3.10.5 and R v.2.2. Key python packages include:
1149 abagen==0.1.3, brainspace==0.1.10, neuromaps==0.0.3. Full details of all packages, a Dockerfile and
1150 link to docker image, and all code used for these analyses are publicly available at
1151 https://github.com/richardajdear/AHBA_gradients.
1152

1153 # Methods-only References

1154 96. Schaefer, A. *et al.* Local-global parcellation of the human cerebral cortex from intrinsic functional
1155 connectivity MRI. *Cereb. Cortex* **28**, 3095–3114 (2018).
1156 97. Destrieux, C., Fischl, B., Dale, A. & Halgren, E. Automatic parcellation of human cortical gyri and
1157 sulci using standard anatomical nomenclature. *Neuroimage* **53**, 1–15 (2010).
1158 98. Desikan, R. S. *et al.* An automated labeling system for subdividing the human cerebral cortex on
1159 MRI scans into gyral based regions of interest. *Neuroimage* **31**, 968–980 (2006).
1160 99. Vos de Wael, R. *et al.* BrainSpace: a toolbox for the analysis of macroscale gradients in
1161 neuroimaging and connectomics datasets. *Commun Biol* **3**, 103 (2020).
1162 100. Coifman, R. R. *et al.* Geometric diffusions as a tool for harmonic analysis and structure definition
1163 of data: diffusion maps. *Proc. Natl. Acad. Sci. U. S. A.* **102**, 7426–7431 (2005).
1164 101. Lafon, S. & Lee, A. B. Diffusion maps and coarse-graining: A unified framework for dimensionality
1165 reduction, graph partitioning, and data set parameterization. *IEEE Trans. Pattern Anal. Mach.*
1166 *Intell.* **28**, 1393–1403 (2006).
1167 102. Kairov, U. *et al.* Determining the optimal number of independent components for reproducible
1168 transcriptomic data analysis. *BMC Genomics* **18**, 712 (2017).
1169 103. Szklarczyk, D. *et al.* STRING v11: protein–protein association networks with increased coverage,
1170 supporting functional discovery in genome-wide experimental datasets. *Nucleic Acids Res.* **47**,
1171 D607–D613 (2018).
1172 104. Yu, C. *et al.* A strategy for evaluating pathway analysis methods. *BMC Bioinformatics* **18**, 453

1173 (2017).

1174 105. Zhang, Y. *et al.* Purification and characterization of progenitor and mature human astrocytes

1175 reveals transcriptional and functional differences with mouse. *Neuron* **89**, 37–53 (2016).

1176 106. Habib, N. *et al.* Massively parallel single-nucleus RNA-seq with DroNc-seq. *Nat. Methods* **14**, 955–

1177 958 (2017).

1178 107. Darmanis, S. *et al.* A survey of human brain transcriptome diversity at the single cell level. *Proc.*

1179 *Natl. Acad. Sci. U. S. A.* **112**, 7285–7290 (2015).

1180 108. Li, M. *et al.* Integrative functional genomic analysis of human brain development and

1181 neuropsychiatric risks. *Science* **362**, (2018).

1182 109. Pirooznia, M. *et al.* SynaptomeDB: an ontology-based knowledgebase for synaptic genes.

1183 *Bioinformatics* **28**, 897–899 (2012).

1184 110. Markello, R. D. *et al.* neuromaps: structural and functional interpretation of brain maps. *bioRxiv*

1185 2022.01.06.475081 (2022) doi:10.1101/2022.01.06.475081.

1186 111. Paquola, C. *et al.* Microstructural and functional gradients are increasingly dissociated in

1187 transmodal cortices. *PLoS Biol.* **17**, e3000284 (2019).

1188 112. Glasser, M. F. *et al.* The minimal preprocessing pipelines for the Human Connectome Project.

1189 *Neuroimage* **80**, 105–124 (2013).

1190 113. Markello, R. D. & Misic, B. Comparing spatial null models for brain maps. Preprint at

1191 https://doi.org/10.1101/2020.08.13.249797.